TOPICAL REVIEW

Magnetic skyrmions: from fundamental to applications

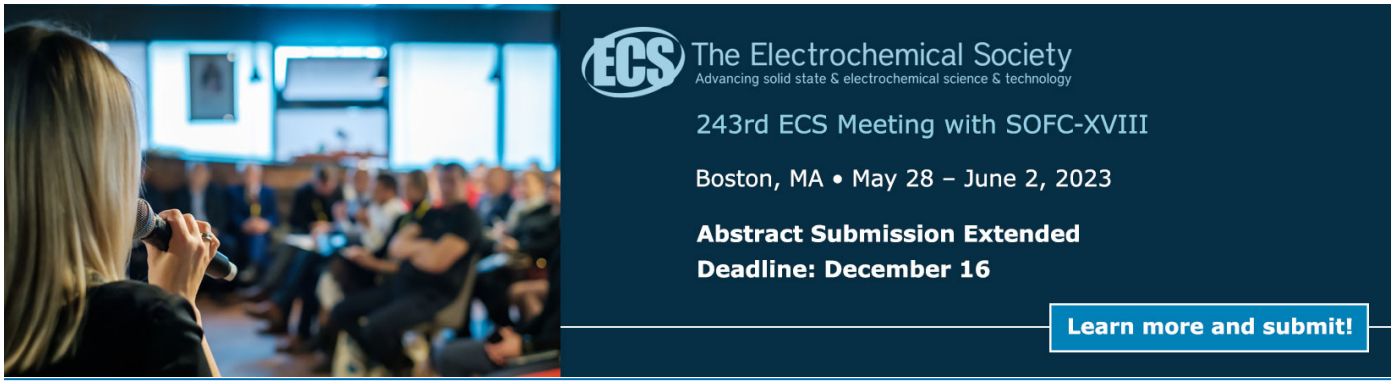

IOP Publishing Journal of Physics D: Applied Physics
J. Phys. D: Appl. Phys. **49** (2016) 423001 (17pp) doi:10.1088/0022-3727/49/42/423001

Topical Review

Magnetic skyrmions: from fundamental to applications

Giovanni Finocchio[1], Felix Büttner[2], Riccardo Tomasello[3], Mario Carpentieri[4] and Mathias Kläui[5,6]

[1] Department of Mathematical and Computer Sciences, Physical Sciences and Earth Sciences, University of Messina, V.le D'Alcontres 31, I-98166 Messina, Italy
[2] Department of Materials Science and Engineering, Massachusetts Institute of Technology, 77 Massachusetts Avenue, Cambridge, MA 02139, USA
[3] Department of Engineering, Polo Scientifico Didattico di Terni, University of Perugia, Terni, TR I-50100, Italy
[4] Department of Electrical and Information Engineering, Politecnico di Bari, via E. Orabona 4, I-70125 Bari, Italy
[5] Institute of Physics, Johannes Gutenberg-Universität Mainz, Staudinger Weg 7, 55128 Mainz, Germany
[6] Graduate School of Excellence Materials Science in Mainz, Staudinger Weg 9, 55128 Mainz, Germany

E-mail: gfinocchio@unime.it

Received 3 May 2016, revised 24 June 2016
Accepted for publication 29 July 2016
Published 22 September 2016

Abstract

In this topical review, we will discuss recent advances in the field of skyrmionics (fundamental and applied aspects) mainly focusing on skyrmions that can be realized in thin film structures where an ultrathin ferromagnetic layer (<1 nm) is coupled to materials with large spin–orbit coupling. We review the basic topological nature of the skyrmion spin structure that can entail a stabilization due to the chiral exchange interaction present in many multilayer systems with structural inversion asymmetry. The static spin structures and the dynamics of the skyrmions are also discussed. In particular, we show that skyrmions can be displaced with high reliability and efficiency as needed for the use in devices. We discuss major possible applications, such as memory, microwave oscillators and logic, and combinations of these, making skyrmions very promising candidates for future low power IT devices.

Keywords: skyrmion, spin-transfer-torque, spin-Hall effect, racetrack memory, microwave oscillator, spin-torque diode effect, logic gates

(Some figures may appear in colour only in the online journal)

1. Introduction to magnetic solitons and their classification

Solitons are self-localized wave packets that can be observed in media characterized by non-linear and dispersive constitutive laws [1–5]. The concept of soliton is very general and can be found in different branches of physics. For instance, the basic equation of nonlinear optics, the nonlinear Schrödinger equation, and the fundamental equation of magnetodynamics, i.e. the Landau–Lifshitz–Gilbert (LLG) equation for isotropic and uniaxially anisotropic magnetic materials, are equivalent, giving rise to similarities between, for instance, nonlinear soliton phenomena in optics and magnetism. In magnetism, a large number of solitons have been studied and observed in experiments, such as (i) domain walls (DWs), that are solitons of the kink type [6–10], (ii) vortices [11–18], (iii) bubbles [19–23] (iv) skyrmions [24–40], etc. In the framework of the conservative LLG equation (Gilbert damping equal to zero) both fixed

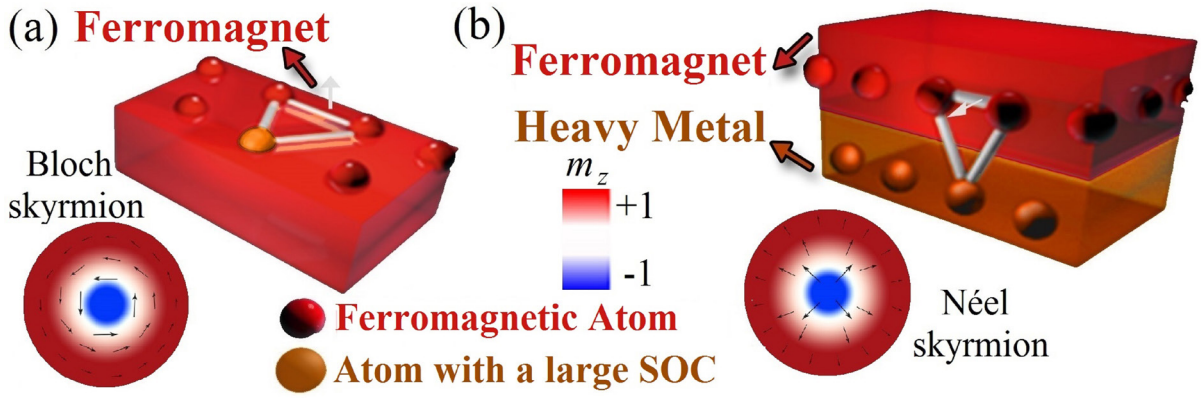

Figure 1. (a) Bulk DMI vector (white arrow) originating in a non-centrosymmetric crystal because of the interaction of the ferromagnetic atoms with an impurity with large SOC. (b) Interfacial DMI vector (white arrow) in a ferromagnet/heavy metal bilayer. The insets represent an example of magnetization distribution for the Bloch and Néel skyrmion. A color scale related to the z-component of the magnetization is also indicated.

points of dynamics (static solitons) or limit cycles (dynamical solitons) can be stabilized, while only static solitons are stable solutions of the non-conservative LLG equation [41–43]. Examples of dynamical solitons are vortex-antivortex pairs [17, 44], droplets [45–50] and dynamical skyrmions [51–53]. The importance of studying these has been highlighted by the experimental evidence that spin-transfer torque (STT) [54] can sustain dynamical states in non-conservative magnetic materials by compensating the Gilbert losses.

A mathematical way to classify solitons is on the basis of their topology, e.g., using the skyrmion number $S = \frac{1}{4\pi}\int n(x,y)\mathrm{d}x\mathrm{d}y$, with $n(x,y)$ being the topological density computed as $\mathbf{m}\cdot(\partial_x \mathbf{m}\times \partial_y \mathbf{m})$, where $\mathbf{m}$ is a vector field (magnetization for ferromagnetic materials) [55, 56]. Topology is a mathematical concept to classify geometrical properties of continuous structures, such as vector fields. Two structures are considered equivalent if a continuous map from one to the other exists. Depending on the physical systems where these solitons are realized, these continuous maps represent transformations that are allowed, while, in continuous systems, other transformations would be prohibited. However, real physical systems are usually discrete, for instance based on the atomistic lattice, which means that other transformations are not completely prohibited, but suppressed. Therefore, energy barriers specify meaningful topological distinctions. In physics, topologies are often classified according to homotopic transformations between spaces with Euclidian metric and an Euclidian definition of neighborhood, and open sets. A homotopy is a continuous deformation, not necessarily bijective. In contrast, homeomorphisms—defining another possible topological classification—are bijective. For instance, a line and a point are homotopically equivalent, but they are not homeomorph. Skyrmions are topological objects according to homotopy transformations. They are homotopic to identity vector fields on a unit sphere, which distinguishes them from the uniform state. The energy barrier separating these topological states is defined by the exchange energy, i.e. the energy required to flip one spin in a uniform environment [57].

In the recent literature, much attention has been given to the investigation of nucleation, stability, manipulation and dynamical properties of topologically protected magnetic solitons, i.e. skyrmions. The skyrmions have been observed in materials with out-of-plane magnetization achieved either with an external field [26, 27, 38–40] or a perpendicular magnetic anisotropy [33–35, 38–40, 53, 58], and are stabilized by means of a trade-off among the exchange and the magnetostatic energy, and the bulk or interfacial Dzyaloshinskii Moriya interaction (DMI) [59, 60]. The bulk DMI is due to a break of the crystal inversion symmetry and the presence of high spin–orbit coupling atoms in a ferromagnetic alloy (for instance B20 materials) [25, 26, 61], while the interfacial DMI (i-DMI) has its origin in the interfaces of a multilayer, where a thin ferromagnetic material is coupled to a large spin–orbit coupling material, such as Pt or Ir. Skyrmions are classified in Bloch or Néel type, where the former is predominantly found in bulk materials, and the latter is characteristic for the i-DMI of multilayers [10, 30, 33, 34]. Their spatial profile is characterized by two out-of-plane domains separated by an in-plane domain wall, which has a circular (clockwise or counter-clock wise) chirality in a Bloch skyrmion, and a radial chirality (inward or outward) in a Néel skyrmion [30, 34]. Usually, the magnetization region going from the geometrical center of the skyrmion inner domain to the one of its domain wall, where the out of-plane component is zero, is identified as skyrmion core. Figure 1 shows the two skyrmion types and a scheme for the bulk and the interfacial DMI. Concerning Bloch skyrmions, they can indeed be stabilized not only by DMI, but also by dipolar interactions (‘bubble skyrmion’). Note that in thin film multilayers, as discussed here, there are always dipolar interactions present. This means that in most cases it is the combination of DMI and dipolar interactions that leads to the stabilization of the observed skyrmion spin structure. So, there are no purely DMI stabilized skyrmions in the thin film multilayers discussed here (unlike in the bulk where dipolar interactions do not play a significant role, which is also the case in the limit approaching zero thickness for the ferromagnetic film). From an experimental point of view, a single snapshot of the spatial profile of a skyrmion with circular chirality is not sufficient to easily distinguish between a Bloch skyrmion, where DMI plays a large role, or bubble skyrmions where DMI is not significant. This difference, however, can be identified with a series of experiments which try

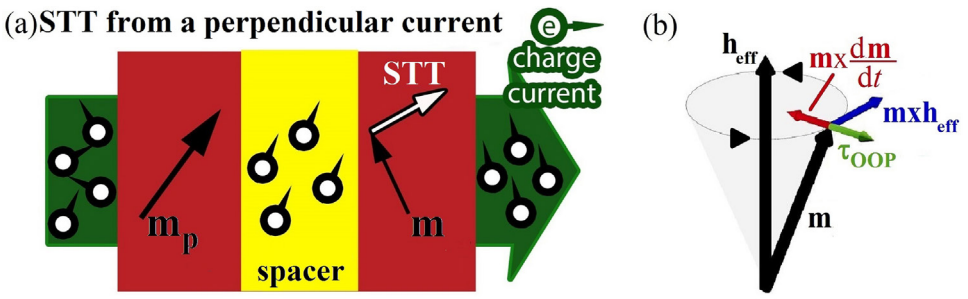

Figure 2. (a) Schematic illustration of the spin-transfer torque exerted on the free layer magnetization in an OOP device. (b) Representation of all the torques acting on the magnetization. Blue is the conservative torque that leads to a Lamor precession around the effective field $\mathbf{h}_{\mathbf{eff}}$. Red is the dissipative Gilbert damping torque that reduces the precession amplitude and eventually leads to a collinear alignment of $\mathbf{h}_{\mathbf{eff}}$ and $\mathbf{m}$. The Slonczewski-like STT (green) is opposite to the Gilbert damping torque, thus realizing an effectively lossless environment for the precessing spin.

to stabilize skyrmions with different circular chirality. If the DMI is sufficiently strong to stabilize only one direction of the DW in the skyrmion, we are dealing with a chiral Bloch skyrmion. Otherwise, if the DMI is smaller so that skyrmions with different circular chirality are stable, then we are dealing with bubble skyrmions (where of course small DMI can still be present). In other words, the soliton is named 'bubble skyrmion' if the DMI is not strong enough to prevent both chiralities from occurring.

In this topical review, while we will mainly focus on the promising applications of skyrmions in ultrathin ferromagnetic materials, and in particular on the single skyrmion stability, nucleation and manipulation, we will also include discussions which are relevant from a fundamental physics point of view. We first give an overview of the micromagnetic framework (section 2) to study the skyrmions properties. Section 3 discusses the basic properties of skyrmions from a theoretical point of view such as size, stability, resonant modes, nucleation, annihilation, and manipulation. Section 4 focuses on recent observations of skyrmions at room temperature and reviews state of the art materials and devices. Section 5 deals with the most promising technological application of skyrmions, i.e. the 'skyrmion racetrack memory' and the required linear displacement of skyrmions in magnetic nanowires. Future perspectives of skyrmion-based devices (microwave detectors and oscillators, and logic) are presented in section 6 including major issues to be overcome. Conclusions are summarized in section 7.

2. Micromagnetic framework for the design and simulation of skyrmion devices

In this section, the detailed micromagnetic framework for the study of skyrmion proprieties is discussed. It includes the DMI formulation and the key information for modeling the driving forces related to the spin-transfer torque and the voltage controlled magnetocrystalline anisotropy that can be used for nucleation, annihilation and manipulation of skyrmions. The last part of the section discusses a collective approach based on Thiele's equation for the description of skyrmion dynamics under the hypothesis of its behavior as a rigid object.

2.1. Basic model

From a theoretical point of view, the static properties of skyrmions can be studied within a micromagnetic framework [62–66] by using the LLG equation [41–43]. The micromagnetic framework predicts the relationship between the spatial distribution of effective magnetic field $\mathbf{h}_{\mathbf{eff}}$ (linked to different energy contributions such as exchange $\mathbf{h}_{\mathbf{exch}}$, anisotropy $\mathbf{h}_{\mathbf{ani}}$, external $\mathbf{h}_{\mathbf{ext}}$, and self-magnetostatic $\mathbf{h}_{\mathbf{M}}$ fields) based on material parameters and the magnetization vector field $\mathbf{m}$. The LLG relates the effective fields to torques τ and links them to the change of magnetization $\mathrm{d}\mathbf{m}/\mathrm{d}t$.

The DMI can be modeled as an additional energetic term to the effective field which acts as an antisymmetric exchange contribution. In fact, while the exchange tries to align adjacent spins in parallel to obtain a uniform magnetization state, the DMI prefers to align them orthogonally, fostering the formation of helical magnetization textures. The energy density in the case of bulk DMI is $\varepsilon_{\mathrm{BulkDMI}} = D\,\mathbf{m}\cdot\nabla\times\mathbf{m}$, whereas the one for the i-DMI, assuming $\frac{\partial \mathbf{m}}{\partial z} = 0$, is $\varepsilon_{i\text{-DMI}} = D[m_z\nabla\cdot\mathbf{m} - (\mathbf{m}\cdot\nabla)m_z]$, with D being the parameter taking into account the intensity of the DMI [67, 68]. The expression of the dimensionless DMI fields are then

$$\mathbf{h}_{\mathbf{BulkDMI}} = -\frac{1}{\mu_0 M_s^2}\frac{\delta\varepsilon_{\mathrm{BulkDMI}}}{\partial\mathbf{m}} = -\frac{2D}{\mu_0 M_s^2}\nabla\times\mathbf{m} \qquad (1a)$$

$$\mathbf{h}_{i\text{-DMI}} = -\frac{1}{\mu_0 M_s^2}\frac{\delta\varepsilon_{i\text{-DMI}}}{\partial\mathbf{m}} = -\frac{2D}{\mu_0 M_s^2}[(\nabla\cdot\mathbf{m})\hat{z} - \nabla m_z] \qquad (1b)$$

where M_S is the saturation magnetization and μ_0 is the vacuum permeability. The DMI also affects the boundary conditions [67] that now hold $\frac{\mathrm{d}\mathbf{m}}{\mathrm{d}n} = \frac{\mathbf{m}\times\mathbf{n}}{\xi}$ and $\frac{\mathrm{d}\mathbf{m}}{\mathrm{d}n} = \frac{1}{\xi}(\hat{z}\times\mathbf{n})\times\mathbf{m}$ for bulk and i-DMI respectively, where $\xi = \frac{2A}{D}$ is a characteristic length and A is the exchange constant. The manipulation of skyrmions, including nucleation and annihilation, can be controlled by the spin-transfer torque (STT) (see figure 2(a)) [54], such as Slonczewski-like STT $\boldsymbol{\tau}_{\mathbf{OOP}}$, achieved when a spin-polarized current $\mathbf{j}_{\mathbf{FE\text{-}oop}}$ flows perpendicularly to the sample plane [69, 70], and in-plane STT $\boldsymbol{\tau}_{\mathbf{IP}}$ [71], when the current flows inside the ferromagnet along the in-plane direction

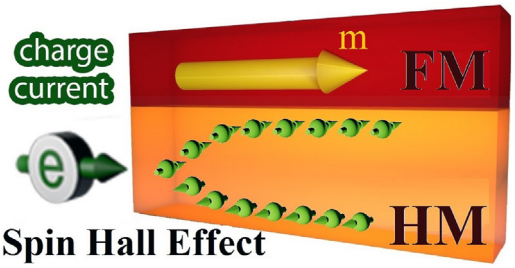

Figure 3. Schematic picture of the FM/HM bilayer, where the SHE arises, inducing opposite spin accumulations near the upper and lower surface of the HM.

($\mathbf{j_{FE\text{-}ip}}$). We wish to underline that we refer to a Cartesian coordinate system where z is the out-of-plane axis, while x and y are the in-plane axes. For in-plane current, we consider a charge current flowing along the x-axis.

2.2. Slonczewski-like spin-transfer torque

The Slonczewski-like STT can be observed in nanopillars or spin-Hall devices [72, 73] and can be modeled as an additional contribution to the LLG equation acting as an anti-damping (see figure 2(b)) [74] as derived by Slonczewski [54]. In nanopillars, the spin-polarization is given by a ferromagnet, named polarizer, with a magnetization $\mathbf{m_p}$. The $\boldsymbol{\tau_{OOP}}$ is given by:

$$\boldsymbol{\tau_{OOP}} = \frac{g\mu_B \mathbf{j_{FE\text{-}oop}}}{\gamma_0 e M_S^2 L_{FM}} \varepsilon(\mathbf{m}, \mathbf{m_p})[\mathbf{m} \times (\mathbf{m} \times \mathbf{m_p})] \qquad (2)$$

with g being the Landé factor, μ_B being the Bohr magneton, e being the electron charge, L_{FM} being the thickness of the ferromagnetic free layer and the polarization function being the $\varepsilon(\mathbf{m_f}, \mathbf{m_p})$, whose expression depends on the relative orientation between the pinned and free layer magnetization, the category of the device (i.e. spin valves, MTJs) and the thicknesses and ferromagnetic materials under investigation. In the case of MTJs, which are the most relevant for applications, the expression of the polarization function is $\varepsilon_{MTJ}(\mathbf{m}, \mathbf{m_p}) = \frac{2\eta}{[1+\eta^2(\mathbf{m}\cdot\mathbf{m_p})]}$, where η is the spin polarization [75]. For MTJs also a voltage-dependent field-like torque should be taken into account [76].

In spin-Hall devices, composed of a bilayer of a ferromagnetic material (FM) and a heavy metal (HM) (see figure 3), the STT originates from the SHE [8, 10, 72, 73, 77–79]. Because of the spin-dependent scattering in the HM, a spin-current is generated from the charge current $\mathbf{j_{HM}}$, giving rise to a spin accumulation of opposite sign at the upper and lower surface of the HM, and then to the STT (see the recent review [80]). The structure of this torque $\boldsymbol{\tau_{SHE}}$ is similar to the Slonczewski torque of equation (2), with the difference that, instead of considering the direction of the spin-polarization given by the magnetization $\mathbf{m_p}$, here the cross product $\hat{z} \times \mathbf{j_{HM}}$ indicates its direction [81–84]:

$$\boldsymbol{\tau_{SHE}} = -\frac{g\mu_B \theta_{SH}}{2\gamma_0 e M_S^2 L_{FM}} \mathbf{m} \times \mathbf{m}(\hat{z} \times \mathbf{j_{HM}}) \qquad (3)$$

with θ_{SH} being the spin-Hall angle, which represents the amount of charge current j_{HM} converted into spin current j_s, $j_s = \theta_{SH} j_{HM}$, and $\hat{z}$ is the unit vector in the out-of-plane direction. Note that this torque assumes that the full spin current is transmitted across the interface and neglects more complex interfacial spin transmission effects.

In addition to the previously discussed SHE-induced torque with a damping-like symmetry, further torques with an orthogonal field-like symmetry can exist. These can result from interfacial effects, such as the inverse spin galvanic effect (ISGE or Rashba Edelstein effect), where electric fields at the interface lead, in the frame of reference of the moving conduction electrons at the interface, to magnetic fields that align the electron spins. These conduction electron spins then act via exchange on the magnetization of the ferromagnetic layer leading, in the simplest picture, to a field-like torque.

The torques that can originate from the SHE or the ISGE are commonly called spin–orbit torques (SOTs) [85, 86]. While originally it was predicted that the ISGE primarily leads to a field-like, and the SHE to a damping-like torque, it is now generally accepted that both can lead to both torques [87, 88], making the analysis more challenging. However, as the dynamics of skyrmions has been predicted to depend primarily on the damping-like symmetry torque, we concentrate on this torque generated by the SHE for this review.

Finally, we note that the transfer of orbital angular momentum overcomes the limit of adiabatic spin transfer torque and allows one to transfer more than $1\hbar$ of angular momentum for each conduction electron.

2.3. In-plane spin-transfer torque

For the current flowing in the ferromagnet, the interaction between the conduction electrons and the magnetization leads to the transfer of spin angular momentum. This has been for a long time the method of choice, for instance, to displace DWs. The in-plane torque $\boldsymbol{\tau_{IP}}$ is composed of two contributions. When crossing a magnetization gradient, the direction of the conduction electron spins adiabatically changes following the local magnetization $\mathbf{m}$ direction, generating the 'adiabatic STT' on $\mathbf{m}$ due to conservation of the total angular momentum. The second STT term, i.e. the non-adiabatic STT, was phenomenologically added in order to explain unexpected early stage experimental results [89]. For details, we refer the reader to an overview of these torques with a theoretical [90] and an experimental focus [91].

2.4. Torque from voltage controlled magnetocrystalline anisotropy

It has been demonstrated in MTJs with an iron rich CoFeB free layer and a MgO spacer that a voltage across the tunnel junction can induce variations of the magnetic anisotropy along the out-of-plane direction, hence inducing dynamics [92–94]. Micromagnetically, this effect is taken into account by considering a voltage-controlled perpendicular magnetocrystalline anisotropy (VCMA), i.e. by modifying the effective field term

related to the anisotropy of the LLG [95]. The VCMA can be used to manipulate the skyrmion motion by inducing a pinning/depenning effect according to the sign of the driving voltage [96].

2.5. Equation of motion for the skyrmion center

Skyrmions are entities with quasi-particle properties. In particular, the trajectory of the center of the skyrmion, defined as the weighted average of the out-of-plane magnetic moment m_z within the area enclosed by the $m_z = 0$ domain wall (skyrmion core), is described by a quasi-particle equation of motion, i.e. the generalized Thiele's equation that derives from the LLG [22, 32–34, 97–99]:

$$-M\ddot{\mathbf{R}} + \mathbf{G} \times (\dot{\mathbf{R}} - \mathbf{u}) - \widetilde{D}(\alpha\dot{\mathbf{R}} - \beta\mathbf{u}) + 4\pi B\widetilde{R}(\psi)\mathbf{j}_{\mathbf{HM}} + \mathbf{F} = 0 \tag{4}$$

Here, $\mathbf{R}$ is the center of mass position and the dots on $\mathbf{R}$ indicate a temporal derivative; $\mathbf{G} = (0, 0, G)$ is the gyrocoupling vector, with the gyrocoupling strength $G = -4\pi SL_{\mathrm{FM}}M_{\mathrm{S}}\gamma_0$; M is the effective mass of the skyrmion; $\widetilde{D} = L_{\mathrm{FM}}M_{\mathrm{S}}\gamma_0 \int \mathrm{d}x\mathrm{d}y(\partial_x \mathbf{m})^2$ is the dissipation constant; $B = \frac{\gamma_0^2 \hbar \theta_{\mathrm{SH}}}{2e} I$, where $\hbar$ is reduced Planck constant, and $I = \frac{1}{4}\int_0^\infty \mathrm{d}r\left(\sin\theta\cos\theta + r\frac{\mathrm{d}\theta}{\mathrm{d}r}\right)$ is a coefficient that depends on the spatial variation of the polar angle θ of the local magnetization orientation; $\widetilde{R}(\psi) = \begin{pmatrix} \cos\psi & \sin\psi \\ -\sin\psi & \cos\psi \end{pmatrix}$ is the rotation matrix corresponding to the domain wall angle ψ that is defined to be 0 for skyrmions with domain wall spins pointing outwards, π for spins pointing inwards, $\pi/2$ for spins rotating counterclockwise, and $3\pi/2$ for spins rotating clockwise; $\mathbf{F}$ is a driving force acting on the skyrmion that has its microscopic origin in a gradient of the out-of-plane effective field. Note that thermal effects, high frequency excitations and gyrodamping are not included in equation (4). These effects are discussed in detail in [100].

3. Fundamental properties

3.1. Stability

Rohart and Thiaville [67] derived a simple analytical expression, which can be used to estimate a critical value D_{C} of the i-DMI parameter at which a single skyrmion in a magnetic dot can be stabilized. The expression valid for ultrathin ferromagnets can be extended to consider the presence of an external field H_Z and a reduced effect of the out-of-plane demagnetizing field $-0.5N_Z\mu_0 M_{\mathrm{S}}$ due to the finite size of the dot (N_Z being the out-of-plane demagnetizing factor):

$$D_{\mathrm{C}} = 4\sqrt{A(K_u + (H_Z - 0.5N_Z\mu_0 M_{\mathrm{S}})M_{\mathrm{S}})}/\pi \tag{5}$$

In a first approximation, D_{C} separates two skyrmion stability regions: for $D < D_{\mathrm{C}}$, the skyrmion diameter d_{sk} (diameter of the skyrmion core) is almost independent of the shape anisotropy (size of the dot) and can be estimated as

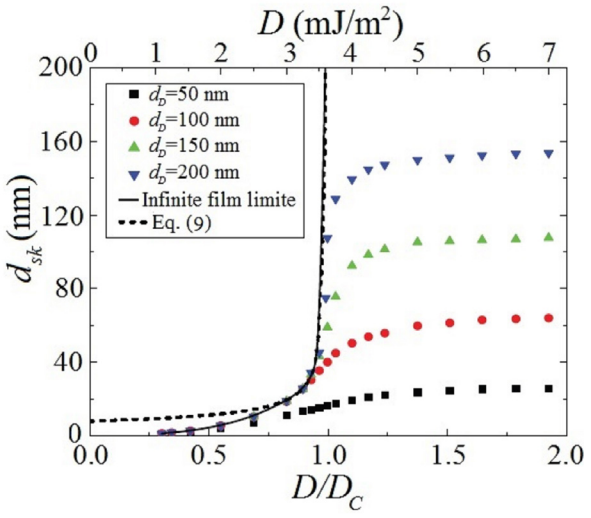

Figure 4. Variation of the skyrmion diameter as a function of D and D_{C} for different dot diameters, as indicated in the legend [67]. The solid line is the solution for an infinite thin film, while the dashed line is the approximate solution of equation (6). Adapted with permission from [67]. Copyright 2016 by the American Physical Society.

$$d_{\mathrm{sk}} = \frac{\sqrt{2A/(K_u + (H_Z - 0.5\mu_0 M_{\mathrm{S}})M_{\mathrm{S}})}}{\sqrt{\left(1 - \frac{D}{D_{\mathrm{C}}}\right)}} \tag{6}$$

For D approaching or being larger than D_{C}, equation (6) is not valid and the skyrmion diameter has to be computed from micromagnetic simulations. We wish to underline that those arguments are still correct for multilayer systems with proper scaling corrections and calculation of stray fields. For $D > D_{\mathrm{C}}$, the confining potential, due to the finite size, can play two roles. Let's consider a dot with a diameter d_{D}. For D approaching D_{C}, the skyrmion diameter tends to be infinite following equation (6), but, as shown by micromagnetic simulations, d_{sk} saturates to a value which depends on d_{D} (see figure 4). However, this behavior is not valid for every d_{D}: as the d_{D} increases, a critical diameter exists at which a single skyrmion is no longer the minimum energetic state, and nucleation of multiple skyrmions in the same dot, i.e. a skyrmion lattice, is the more energetically favorable configuration.

Some open challenges are the development of an analytical theory which takes into account the effect of the confining potential for skyrmion stability and size and the effect of stray fields.

3.2. Nucleation and annihilation

Several procedures have been investigated to nucleate skyrmions. As predicted by Zhou *et al* [101] and demonstrated experimentally by Jiang *et al* [37] in Ta/CoFeB/MgO trilayers, Néel skyrmions can be obtained through a conversion of domain walls (DWs) driven by the SHE in a symmetrically designed wire containing a geometrical constriction. This configuration yields a non-uniform distribution of the current around that narrow neck. When the current is applied, the domains pass through the constriction and are converted into skyrmions at the end of the neck (see figures 5(a) and

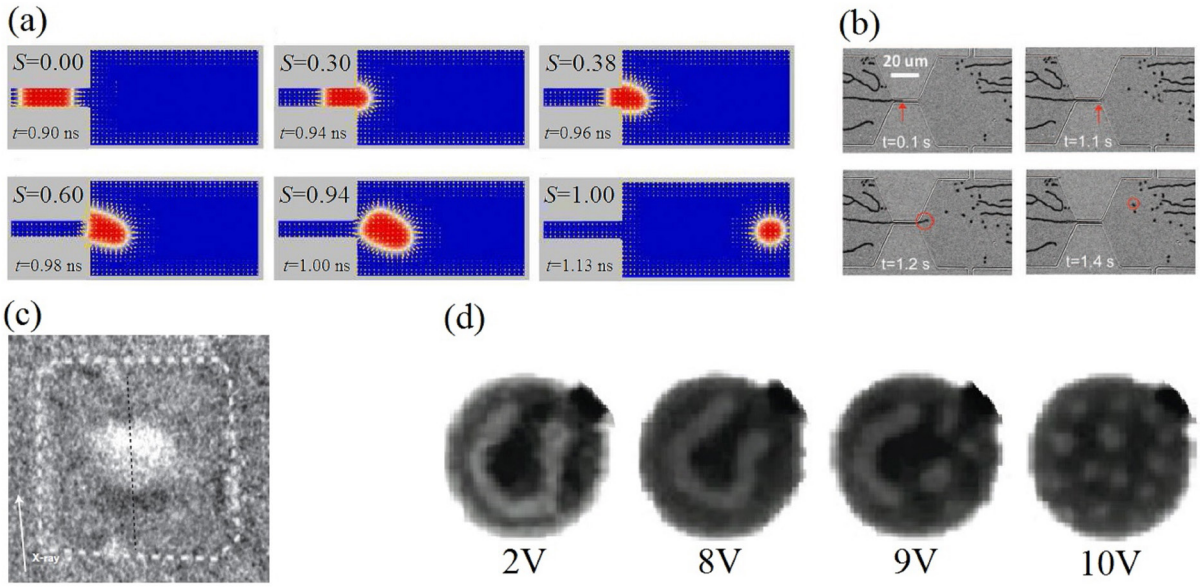

Figure 5. (a) Micromagnetic predictions of the Néel skyrmion nucleation via a DW conversion. The colors are linked to the z-component of the magnetization (blue negative, red positive). The skyrmion number and the times are also indicated in each snapshot from [101] the Nature Publishing Group, copyright 2014. (b) Experimental evidence of the Néel skyrmion nucleation via a DW conversion from [37]. Reprinted with permission from AAAS, Copyright 2015. (c) Image of a 420 nm square dot, where a single Néel skyrmion is nucleated. Reproduced by permission from Macmillan Publishers Ltd [39], Copyright 2016. (d) Néel skyrmions lattice obtained after applying a 10 V bipolar pulse [40]. Reproduced with permission from the Nature Publishing Group, Copyright 2016.

(b)). This mechanism resembles the development of bubbles from soap films by blowing air via a straw. For this reason, the process is known as 'blowing skyrmion'.

Later, the nucleation in Ir/Co/Pt [38], and Pt/Co/MgO [39] multilayers has been experimentally demonstrated as well (see figure 5(c)). In the former, skyrmions were obtained by increasing the out-of-plane external field starting from a multi-domain state, in the latter by decreasing the external field, starting from the out-of-plane saturation state. In particular, Boulle *et al* [39] observed a single skyrmion at zero external field.

Finally, skyrmions have been nucleated by means of increasing the out-of-plane external field pulses starting from labyrinth stripe domain [40]. Over a critical value of the external field (corresponding to voltage of 10 V applied in that experiment), the stripe domain breaks into a geometrically confined skyrmion lattice (see figure 5(d)).

However, the control of the room temperature nucleation of a single skyrmion is still an open challenge. Up to date, single skyrmions have been experimentally nucleated near zero temperature by means of spin-polarized scanning tunneling microscope [102, 103] in perpendicularly magnetized ultrathin films.

Numerical works have shown the possibility to nucleate a single skyrmion via different methods. Iwasaki *et al* [32] simulated a notch in the perpendicularly magnetized wire, and, by applying an electric current pulse, nucleated a Bloch skyrmion from the notch via the spin-transfer torque. A similar shape-assisted process combined with a microwave field can be also used, as predicted by Ma *et al* [104]. In the milestone work by Sampaio *et al* [33], a single skyrmion was created in a micromagnetic simulation by means of the STT from an out-of-plane spin-polarized current locally injected perpendicularly to an out-of-plane ultrathin film (see figure 2 in [33]). Eventually, a nucleation process driven by a pure spin current (use of the spin–orbit

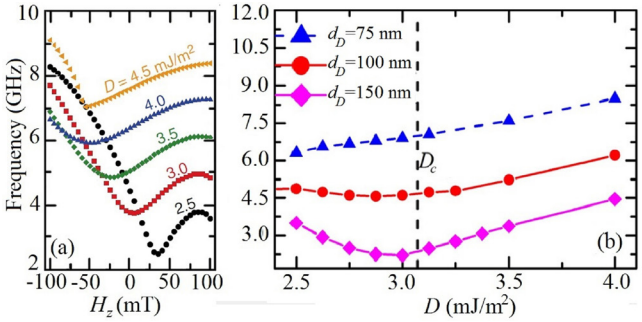

Figure 6. Ferromagnetic resonance frequency of the breathing mode of the Néel skyrmion excited by (a) ac perpendicular external field, for different values of the i-DMI parameter [107], and (b) ac current, for three values of the dot diameter [108]. Adapted with permission from [107]. Copyright 2016 by the American Physical Society and adapted from [108] with permission of AIP Publishing.

torque from the spin-Hall effect) has been proposed to control the nucleation of single skyrmions. In this case, the mechanism is also mediated by the generation of spin-waves [105].

On the other hand, skyrmions can be annihilated by applying either large enough out-of-plane external fields or dc perpendicularly spin-polarized current [102]. In particular, the external field, in the former, and the spin-polarization, in the latter, have to be opposite to the direction of the skyrmion core. But again, addressing individual skyrmions without affecting other skyrmions in the vicinity in a real device remains a technological challenge.

3.3. Resonant modes

As response to external weak perturbations, a skyrmion can be deformed with a deformation degree that is governed by its

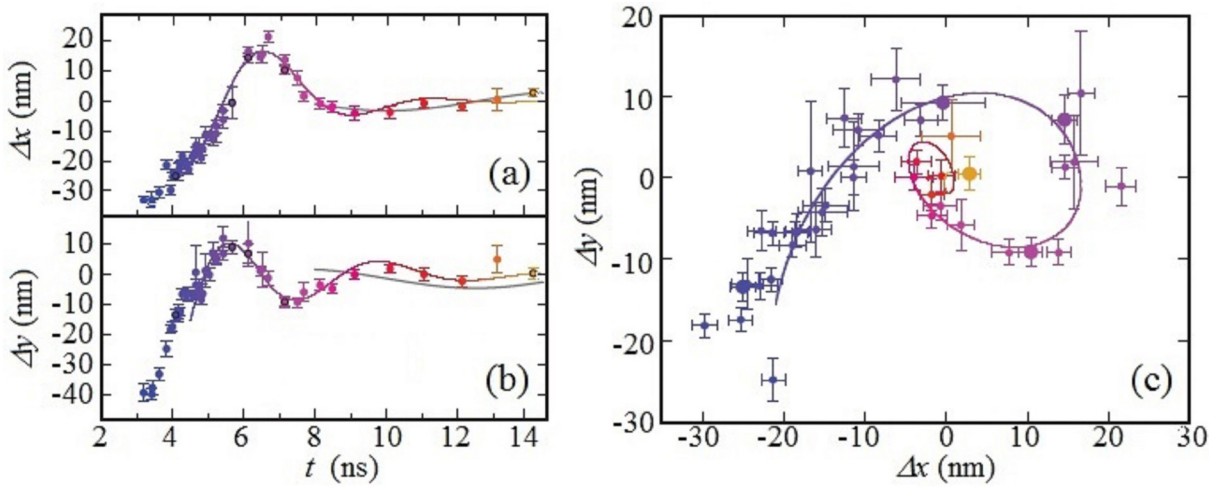

Figure 7. Experimentally observed spiraling motion of a skyrmion moving in a parabolic potential from [36] the Nature Publishing group, Copyright 2015. The plots in (a) and (b) show the time domain evolution of the center coordinates x and y of the skyrmion respectively, while the panel (c) shows the x-y trajectory of the center coordinate considering the data in (a) and (b). The colored lines represent a fit to the data with equation (7). The gray line represents a fit with equation (4) where the mass was set to zero, which is obviously not able to describe the data directly demonstrating the finite mass for these skyrmions.

internal modes. Lin *et al* [106], by using a perturbation theory, have identified different modes associated to the deformation of the skyrmion domain wall and a uniform breathing mode. Makhfuz *et al* [22] have associated the deformation of the skyrmion with waves propagating along the domain wall and have suggested that the skyrmion mass can be derived from the Döring mass of the domain wall, which was used to show experimentally that skyrmions can exhibit large effective masses [36], as detailed below. For applications, it is important to understand those modes that were studied in confined ultrathin circular dots.

Kim *et al* [107] micromagnetically analyzed the dynamical properties of a single Néel skyrmion excited by a microwave perpendicular field in a circular dot. Three main different modes can be identified. The first one is a breathing mode of the skyrmion core, i.e. the skyrmion continuously shrinks and expands, while preserving its radial symmetry, giving rise to a persistent oscillation of the out-of-plane magnetization component. This mode exhibits a much lower frequency than the ferromagnetic resonance (FMR) mode in the uniform case. The second and third modes are a hybridization between the breathing mode and a radial spin-wave mode, with also an excitation at the sample boundaries. The last two modes are characterized by frequencies close to the one of the FMR mode for the uniform magnetic state. The analysis of those modes suggests that the presence of a skyrmion is linked to a low-frequency excitation.

The most relevant mode for applications is the uniform breathing mode. Kim *et al* [107] studied the effect of the perpendicular external field on the breathing mode resonance frequency, for different values of the DMI parameter. As it can be seen, the resonance frequency exhibits a non-monotonic trend as a function of the DMI (see figure 6(a)). Similar results are achieved if the excitation source is a microwave current [108]. Again, the skyrmion is characterized by a uniform breathing mode and a non-monotonic trend of the resonance frequency (see figure 6(b)). Finocchio *et al* [108] micromagnetically demonstrated that this behavior is linked to the critical DMI value D_C. When D is below D_C, the confining force is negligible, whereas for D near or above D_C, the confining force fixes the skyrmion size. Therefore, in the samples with small enough lateral dimensions to obtain a predominance of the confining force on the skyrmion, the FMR frequency versus D exhibits a monotonic trend. When the sample is larger, the confining force is negligible at low D, leading the ascendant monotonic trend to start close to D_C.

The presence of the gyro vector in equation (4) leads to a spiraling motion of a skyrmion when it is excited in a parabolic potential (see figure 7). This gyration has been studied numerically by Moutafis *et al* [55] with a subsequent theoretical interpretation of the result provided by Makhfudz *et al* [22]. Essentially, due to the skyrmion inertia, two gyrotropic modes exist: one where the skyrmion is spiraling clockwise and one where it is spiraling counter-clockwise. This is in contrast to the well-studied gyration of magnetic vortices. The two gyrotropic modes usually have different amplitudes and different damping. Skyrmion gyrations have been experimentally detected by Onose *et al* [109], Schwarze *et al* [110] and observed directly by Büttner *et al*., [36]. Further theoretical studies on the subject of skyrmion gyration were published by Mochizuki [111] and Moon and coworkers [112].

4. Observation of skyrmions

Bubble skyrmions have been investigated for decades, and many of their properties, such as the gyro force, are associated with their topology and hence are universal [113]. Recent experiments have focused on investigating the details of skyrmion spin structure [27, 28, 114], skyrmion lattices [26, 27, 115, 116], high frequency dynamics of skyrmions [36, 109], their stability [38, 39, 103, 117, 118], creation [37, 102], and annihilation [102] in thin films and DMI-dominated bulk materials, as well as on their interaction with spin currents [29, 37, 40, 119–123].

One of the main advantages of using materials with strong DMI is that circular domains in such materials have a well-defined $|S| = 1$ skyrmion number and a fixed chirality. If two such skyrmions merge there are two possibilities. Theoretically, a spin structure with $|S| = 2$ could result. However, in systems with sufficient DMI, this is not stable, so the total skyrmion number reduces from $|S| = 2$ to $|S| = 1$ via a propagation of a hedgehog Bloch point along a vertical Bloch line, where the Bloch point has magnetic monopole properties [122]. It was recently observed that such mergers occur if one of the two skyrmions is pinned, which hints that, for instance, local reduction in the DMI (which pins skyrmions) allows for such mergers to occur more easily, while generally the merging with a change in the topology and thus skyrmion number is suppressed [40]. In large bubbles without DMI, in contrast, vertical Bloch lines are typically stable, and up to $|S| = 90$ skyrmion numbers have been observed [113]. Simulations [55] and experiments [114] report the existence of $|S| \neq 1$ bubble skyrmions in materials without sizeable DMI even when the skyrmion radius is in the sub-200 nm regime, whereas, to the best of our knowledge, no such reports exist for skyrmions in materials with large DMI, as the DMI strongly favors $|S| = 1$ skyrmions. Therefore, the presence of DMI stabilizes the skyrmion topology and the experimental observation of chiral skyrmions is a major advantage for the stability and thus for full control over skyrmions.

The first observation of chiral skyrmions was achieved by Mühlbauer *et al* by neutron scattering [26] and by Yu *et al* via real space transmission electron microscopy imaging [27]. These experiments were carried out at a low temperature of less than 40 K. Room temperature observation of chiral skyrmions has been reported much more recently [37–40, 58, 123], where all these studies commonly report on Néel skyrmions in thin film multilayers.

Beyond the question of creation and stability, the properties of skyrmions have been studied in a few recent experiments, including (i) the field-dependence of the skyrmion diameter [103], (ii) the observation of the skyrmion gyrotropic motion [36], (iii) the measurement of the skyrmion Hall angle [121, 123], and (iv) the determination of the critical current density for moving skyrmions [29, 40, 120]. We will briefly review those experiments subsequently.

Measurements of the field-dependent size of skyrmions were performed with single spin resolution using scanning tunneling microscopy with a spin-polarized tip (SP-STM) [103]. One of the main results of the study is that spin configuration of a skyrmion can be mathematically described by a superposition of two domain walls. Specifically, in cylindrical coordinates r, φ, z, the spin angle ψ, with respect to the radial unit vector, is constant (equal to the previously defined domain wall angle) and the spin angle θ, with respect to the z-axis, is a function of the radial coordinate via:

$$\theta(r, R_0, \Delta) = \theta_{\mathrm{DW}}(r - R_0, \Delta) + \theta_{\mathrm{DW}}(r + R_0, \Delta) \quad (7a)$$

$$\theta_{\mathrm{DW}}(r, \Delta) = 2 \arctan\left[\exp\left(\frac{r}{\Delta}\right)\right] \quad (7b)$$

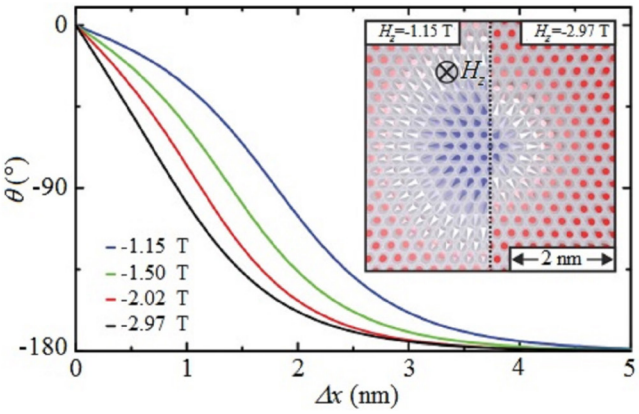

Figure 8. Radial profile of the spin angle θ of a skyrmion as a function of magnetic field from [103]. Reproduced with permission from the American Physical Society, Copyright 2015. The radius of the skyrmion increases continuously with increasing the amplitude of the magnetic field, while the domain wall width is approximately constant.

The parameter R_0 describes the transition between skyrmions with a point-like core and skyrmions with an extended core. While some theoretical papers claim a fundamental difference between the two [124, 125], the work by Romming *et al* indicates that R_0 is a continuous parameter as a function of field without any sign of a phase transition (see figure 8) [103]. However, the range of continuously changed parameters R_0 is too small to conclusively answer whether fundamental classifications of skyrmions based on details of the radial profile are valid or not.

The gyrotropic motion of skyrmions is a direct consequence of the generalized Thiele's equation [97]. When a skyrmion is placed in a parabolic potential $\mathbf{F} = -K\mathbf{R}$, the relaxation to the $\mathbf{R} = 0$ ground state occurs via a spiraling motion due to the gyro force $\mathbf{G} \times \dot{\mathbf{R}}$. While the effect of the gyro force was investigated several decades ago in the linear motion of skyrmions [113], the spatial and temporal resolution to investigate the spiraling relaxation has only recently become available. In the pioneering experiment, a Bloch skyrmion in a material without DMI was displaced and the relaxation in the material's natural pinning potential was directly observed [36]. The imaging technique, x-ray holography, is based on Fourier space imaging and the real space reconstruction of the magnetic image is insensitive to sample drift [116]. Hence, the skyrmion could be tracked with a precision of better than 3 nm, facilitating the conclusion that the trajectory is a superposition of a clockwise and a counter-clockwise spiral. The existence of these two modes demonstrates that the skyrmion has intrinsic inertia. A detailed analysis showed that the mass of the skyrmion is much larger than the well-known mass resulting from the inertia of its domain wall [22], a phenomenon that was attributed to the ability of the skyrmion to absorb or release energy via its breathing mode [36]. The gyrotropic resonances have been further studied spectroscopically and possible applications in tunable gigahertz resonators have been suggested [109, 110].

The skyrmion Hall angle, i.e. the angle ξ between the skyrmion trajectory and a constant excitation, was previously

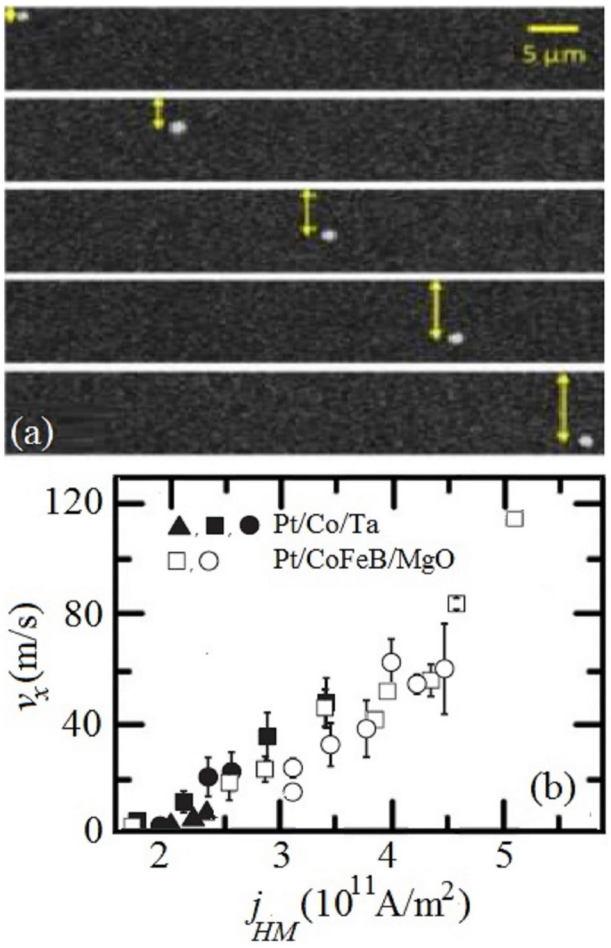

Figure 9. (a) Images of time evolution of the Néel skyrmion motion induced by the SHE in Ta/CoFeB/TaO_x, where the transversal motion is clearly observed from [121] under the CC BY 4.0 license. (b) Experimental velocity–current relation for Néel skyrmion moved by the SHE [40]. Reproduced with permission from the Nature Publishing Group, Copyright 2016.

investigated for skyrmion motion driven by magnetic field gradient forces [113]. Specifically, it was found that for a constant force **F**,

$$\tan(\xi) = -\frac{2S\Delta_0}{r_{sk}\alpha}, \tag{8}$$

where Δ_0 is the domain wall width parameter of the skyrmion domain wall and r_{sk} is the skyrmion radius. Fundamentally, the current-induced spin Hall term in the extended Thiele's equation is identical to a force excitation, i.e. the same skyrmion Hall angle is expected. However, Yu *et al* found some deviation from the simple prediction of equation (8), which they explain by the manifold interactions of currents with the magnetization, i.e. via (i) spin injection due to the spin Hall effect, (ii) direct spin torque, and (iii) Oersted fields [123]. In a more recent study, Jiang *et al* observed that the skyrmion Hall angle (see figure 9(a)) depends on the strength of the excitation relative to the pinning strength in the material [121]. In particular, when the pinning is dominant, i.e. in the so-called creep regime, the skyrmion Hall angle is varying and on average is almost zero. For increasing driving force, i.e. when approaching the flow regime, the skyrmion Hall angle increases linearly with the driving force. The authors anticipate that the skyrmion Hall angle saturates at the theoretical value given by equation (8), but experimental demonstration of this theoretical prediction remains elusive.

Finally, experiments have shown that lattices of skyrmions in single crystal materials can be moved by in-plane spin transfer torques at ultralow current densities of 10^6 A m^{-2}, which is about five to six orders of magnitude lower than the critical current density required to move straight domain walls [29, 120, 126]. This observation has become one of the main motivations for application-oriented skyrmion research. Micromagnetic simulations showed that skyrmions in infinite films do not experience the effect of intrinsic pinning known for domain walls [127]. Also, the critical current density for moving skyrmions in simulations that include pinning was found to be lower than for domain walls in the same material, but only by one order of magnitude, indicating that part of the reason for the observed ultralow critical current densities is the small pinning in the epitaxial materials. Moreover, further micromagnetic simulations suggest that skyrmions in wires, once they feel the repulsive potential of the wire edge, show the same effect of intrinsic pinning as domain walls. However, in multilayers at room temperature, critical current densities for moving isolated skyrmions of 6×10^9 A m^{-2} [121], 10^{10} A m^{-2} [123], and 2×10^{11} A m^{-2} [40] have been measured (see figure 9(b)). Those experiments were conducted in wires, but the skyrmions were far away from the edges and the results are expected to resemble the motion of skyrmions in infinite films. Moreover, it should be noted that the skyrmions in thin film multilayers were moved by exploiting the SHE in the non-magnetic layers, which is expected to be significantly more efficient than the in-plane spin transfer torque used to move skyrmions in epitaxial materials [33, 34]. To what extent the increased critical current densities in multilayers should be attributed to the larger pinning of the material or to different behavior of isolated skyrmions compared to skyrmion lattices remains to be investigated. The subsequent section discusses the motion of skyrmions in wires in more detail.

5. Current-driven skyrmion motion

Over the past four years, the manipulation of skyrmions via an in-plane current has been intensely investigated both theoretically and numerically and, very recently, also experimentally for application in racetrack memory. The earliest studies involved Bloch skyrmions. In 2012, Yu *et al* [126] showed the current-induced motion of a Bloch skyrmion lattice using Lorentz microscopy, while Schulz *et al* [29] and Everschor *et al* [128] theoretically analyzed the skyrmion motion using Berry phase arguments and Thiele's equation [97], respectively. Those works confirmed that skyrmions could be driven by the same in-plane STT mechanism (see section 2.3) as DWs. The first numerical experiment was performed by Iwasaki *et al* [127] on a Bloch skyrmions lattice moved by the in-plane STT in an infinite MnSi film, obtaining the following main results: skyrmions exhibit lower depinning currents than helix phase, are insensitive to defects, and are characterized by two velocity components (parallel and perpendicular to the direction of the electric current). If the Gilbert damping α is equal to the

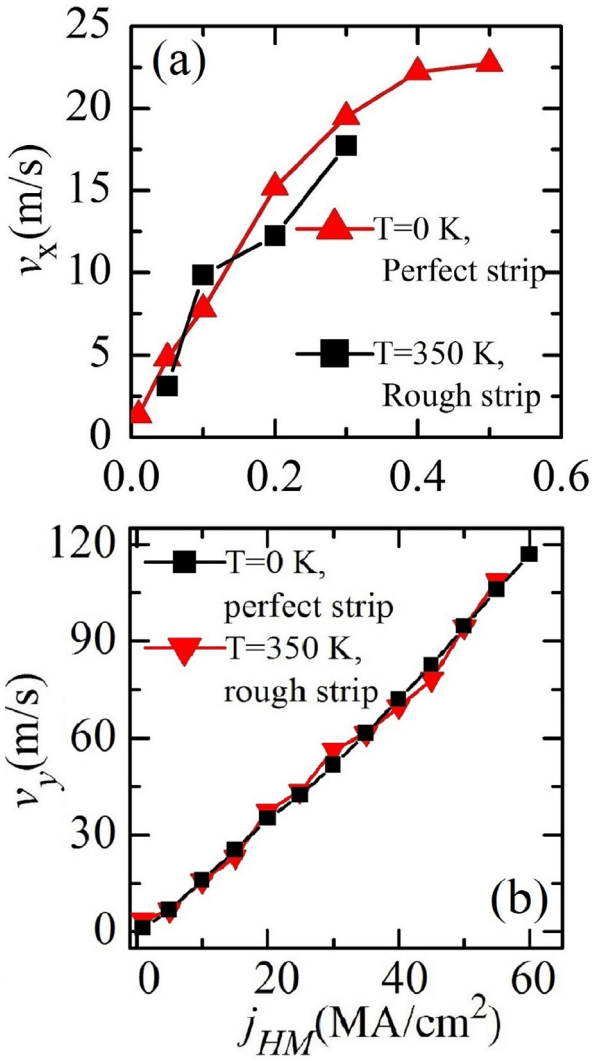

Figure 10. (a) Velocity–current relation for the Néel skyrmion moved by the SHE [34] in the scenario proposed by Sampaio *et al* [33]. (b) Velocity–current relation for the Néel skyrmion moved by the SHE along the direction perpendicular to the electrical current [34]. Adapted from [34] with permission from the Nature Publishing Group, Copyright 2014.

non-adiabatic parameter of the STT β, the skyrmions exhibit only the parallel velocity component. The velocity–current relation becomes 'universal', meaning that the parallel velocity does not depend on the β/α ratio and defects, contrarily to the helix one. The same group later showed [32] the motion of a single Bloch skyrmion in a wire. Differently from the lattice, the single skyrmion motion induced by the STT is strongly influenced by the β/α ratio as well as by defects. This difference is ascribed to a repulsive potential arising near the sample edges and linked to the DMI boundary conditions. In particular, when $\beta = 0$, the skyrmion velocity drops to zero after an initial motion, whereas if $\beta \neq \alpha$, the skyrmion exhibits a non-zero velocity component perpendicular to the electric current direction. This is linked to the so-called Magnus force, leading to the skyrmion Hall effect. Besides, because of the repulsive potential, a critical value of the current exists over which the skyrmion is expelled from the wire. In other words, when the force due to the spin-transfer torque overcomes the one from the boundary, the skyrmion annihilates at the sample edges; on the other hand, when the force is low, the skyrmion is bounced back.

The first numerical demonstration of Néel skyrmion motion was proposed by Sampaio *et al* [33] in a perpendicular ultrathin ferromagnetic strip. By means of micromagnetic simulations, they proved that also the Néel skyrmion can be shifted via the in-plane STT, and, similarly to the Bloch skyrmion, exhibits two velocity components if $\beta \neq \alpha$, whereas the motion is longitudinal when $\beta = \alpha$. In the same work it was also shown that Néel skyrmions can be driven by the SHE in ferromagnet/heavy metal bilayers. That mechanism induces the motion along the same direction of the current injected into the heavy metal and it is energetically more efficient than the in-plane STT, as the same skyrmion velocities can be achieved by applying lower currents (see figures 3(a) and 10(a) in [33]). Tomasello *et al* [34] micromagnetically studied four possible scenarios obtained by combining the skyrmion type (Néel and Bloch) and the motion source (STT and SHE), highlighting that Néel skyrmions driven by the SHE mainly move in the direction perpendicular to the electric current (see figure 10(b)). That scenario is characterized by a technological limit owed to the transient breathing mode excited as soon as the current is applied. Over a threshold value of the applied current, the skyrmion critically expands and touches the sample boundaries. However, if the current is small enough in order that the SHE force is balanced by the repulsive force from the sample boundaries, the skyrmion moves in the same direction of the electric current, as proposed by Sampaio *et al*. The scenario in [34] is more robust to thermal fluctuations at room temperature and surface/edge roughness (see figure 10(b)), as well as allowing to achieve larger skyrmion velocities, whereas the scenario in [33] can be useful for ultralow power applications.

Very recently, the SHE-induced motion of Néel skyrmions in synthetic antiferromagnets (SAF) due to a damping-like symmetry spin orbit torque has been numerically demonstrated [129]. The SAF framework, where a thin Ruthenium (Ru) layer is sandwiched between two ferromagnets, was introduced by Yang *et al* [130] for the experimental study of DW motion driven by the SHE. A SAF is characterized by the interlayer exchange coupling (IEC) [131], whose sign depends on the thickness of the Ru layer. Negative values of the IEC constant favor an antiferromagnetic alignment of the magnetization of the two ferromagnets. With this in mind, a possible configuration of the skyrmion based SAF includes a skyrmion with a negative core and outward chirality in the lower ferromagnet, and a skyrmion with a positive core and inward chirality in the upper ferromagnet. The very important feature of skyrmions motion in SAFs is that they exhibit only a longitudinal velocity along the current flow since the IEC couples both skyrmions in the two layers and, thus, the opposite Magnus force cancels (see figures 11 and 17). Therefore, it is possible to achieve velocities one order of magnitude larger (see figure 11) with respect to skyrmions in single ferromagnet/heavy metal bilayers [129].

Recently, the displacement of Néel skyrmions has been experimentally observed. It has been demonstrated in extended Ta/CoFeB/MgO multilayers [37], even in presence of perpendicular anisotropy gradients [123], and the motion

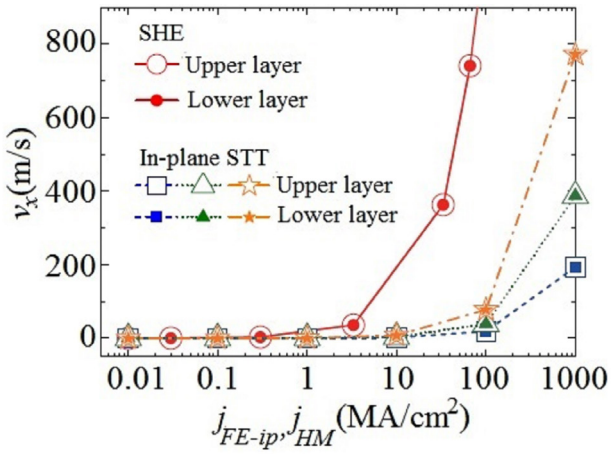

Figure 11. Velocity–current relation related to the SHE- and in-plane STT-induced motion for coupled Néel skyrmions in a SAF racetrack memory from [129] the Nature Publishing Group, Copyright 2016.

has been detected in smaller Pt/Co/Ta wires [40]. However, those experimental findings are partly in contrast with theoretical and numerical predictions. For instance, the skyrmions move at higher critical currents, the angle with respect to the electric current does not fit simple theory and simulations, and the skyrmions seem to be influenced by pinning, as described in section 4. So, here are open questions that show that this developing field holds promise for a number of further discoveries and a deeper understanding of the effects.

6. Skyrmion based microwave detectors and oscillators, and logic

6.1. Microwave detectors

Recent micromagnetic results have predicted the possibility to use magnetic skyrmions for the design of microwave detectors with high sensitivities larger than 2000 V W^{-1} for optimized contact diameters [108]. Microwave detectors are based on the spin-transfer torque diode (STD) effect, which is a rectification effect that converts a microwave current into a dc voltage [94, 132–139]. The physics at the basis of the STD effect is linked to the excitation of the ferromagnetic resonance, which is obtained when an input microwave current $i_{\mathrm{MTJrf}} = I_{\mathrm{M}} \sin(2\pi f_{\mathrm{rf}} t + \varphi_{\mathrm{I}})$ is passed by an MTJ with a frequency f_{rf} close to the ferromagnetic resonance frequency f_0. The free layer magnetization starts to oscillate because of the STT and, consequently, the magnetoresistive effect related to the tunneling magnetoresistance converts this oscillation into a resistance oscillation $r = \Delta R_{\mathrm{S}} \sin(2\pi f_{\mathrm{rf}} t + \varphi_{\mathrm{R}})$. Coupling the input microwave current to the oscillating resistance, the output voltage v_{out} is obtained $v_{\mathrm{out}} = i_{\mathrm{MTJrf}} \cdot r = I_{\mathrm{M}} \Delta R_{\mathrm{S}} \sin(2\pi f_{\mathrm{rf}} t + \varphi_{\mathrm{I}}) \sin(2\pi f_{\mathrm{rf}} t + \varphi_{\mathrm{R}})$. Making some calculations, the following expression is reached:

$$v_{\mathrm{out}} = \frac{1}{2} I_{\mathrm{M}} \Delta R_{\mathrm{S}} \left[\cos(\varphi_{\mathrm{I}} - \varphi_{\mathrm{R}}) - \cos(4\pi f_{\mathrm{rf}} t + \varphi_{\mathrm{I}} + \varphi_{\mathrm{R}})\right] \tag{9}$$

which gives rise to the following dc component of the voltage (rectification voltage):

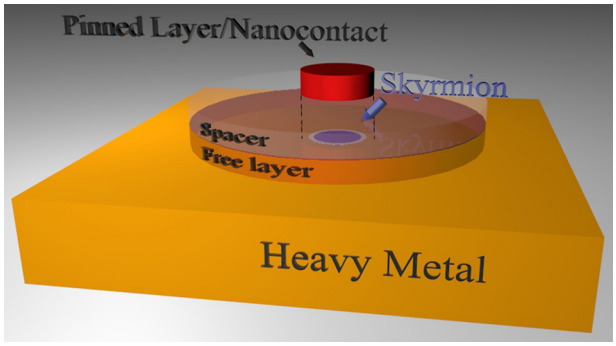

Figure 12. Sketch of the device involving an MTJ and a skyrmion for the study of the skyrmion based STD.

$$V_{\mathrm{dc}} = \frac{1}{2} I_{\mathrm{M}} \Delta R_{\mathrm{S}} \cos(\Phi_{\mathrm{S}}) \tag{10}$$

where $\Phi_{\mathrm{S}} = \varphi_{\mathrm{I}} - \varphi_{\mathrm{R}}$ represents the phase difference between the input current and the resulting oscillating resistance.

One of the most significant parameters, which can be seen as a figure of merit for the STD efficiency in converting an input power into a usable voltage, is the sensitivity. This represents the conversion of the microwave input power P_{in} into the output dc voltage V_{dc}:

$$\varepsilon = \frac{V_{\mathrm{dc}}}{P_{\mathrm{in}}} \tag{11}$$

The structure used to investigate the skyrmion based STD effect is an MTJ with a perpendicular polarizer patterned as nano-contact (diameter d_{C}) for a local injection of the current and the free layer coupled to a heavy metal, in order to give rise to a large enough *i*-DMI to obtain a skyrmion as ground state [108] (see figure 12).

As described in section 3.3, the skyrmion response to a microwave current is mainly characterized by the excitation of a uniform breathing mode that induces a resistance oscillation of an amplitude, linked to the minimum and maximum skyrmion core diameter $d_{\mathrm{sk\text{-}min}}$ and $d_{\mathrm{sk\text{-}max}}$, given by

$$\Delta R_{\mathrm{S}} = \begin{cases} (R_{\mathrm{AP}} - R_{\mathrm{P}}) \dfrac{d_{\mathrm{sk\text{-}max}}^2 - d_{\mathrm{sk\text{-}min}}^2}{d_c^2} & d_{\mathrm{sk\text{-}max}} < d_{\mathrm{C}} \\ (R_{\mathrm{AP}} - R_{\mathrm{P}}) \left(1 - \dfrac{d_{\mathrm{sk\text{-}min}}^2}{d_{\mathrm{c}}^2}\right) & d_{\mathrm{sk\text{-}max}} \geqslant d_{\mathrm{C}} \end{cases} \tag{12}$$

with R_{AP} and R_{P} being the antiparallel and parallel resistance of the MTJ. The value of ΔR_{S} is as large as $d_{\mathrm{SK\text{-}min}}^2 \to 0$ and $d_{\mathrm{SK\text{-}max}} \to d_{\mathrm{C}}$ simultaneously.

Figure 13 summarizes the sensitivities computed for different current amplitudes, input powers and contact sizes ($R_{\mathrm{AP}} = 1500\ \Omega$ and $R_{\mathrm{P}} = 1000\ \Omega$) [140]. One key finding is the existence of an optimal contact size where the sensitivity exhibits a maximum value of about 2000 V W^{-1}.

6.2. Spin transfer nano-oscillator

The possibility to design spin-transfer nano-oscillators [70] in presence of a large enough *i*-DMI has been experimentally, micromagnetically, and analytically analyzed [51–53]. Firstly,

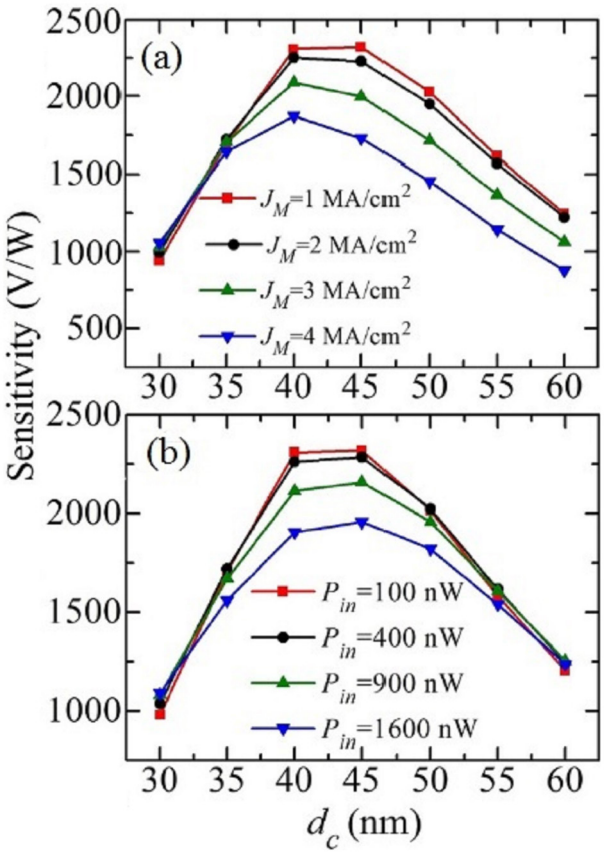

Figure 13. Sensitivity as a function of the contact diameter for different (a) amplitudes of the microwave current and (b) input microwave powers, as indicated in the legend [108]. Adapted from [108] with permission from AIP Publishing, Copyright 2015.

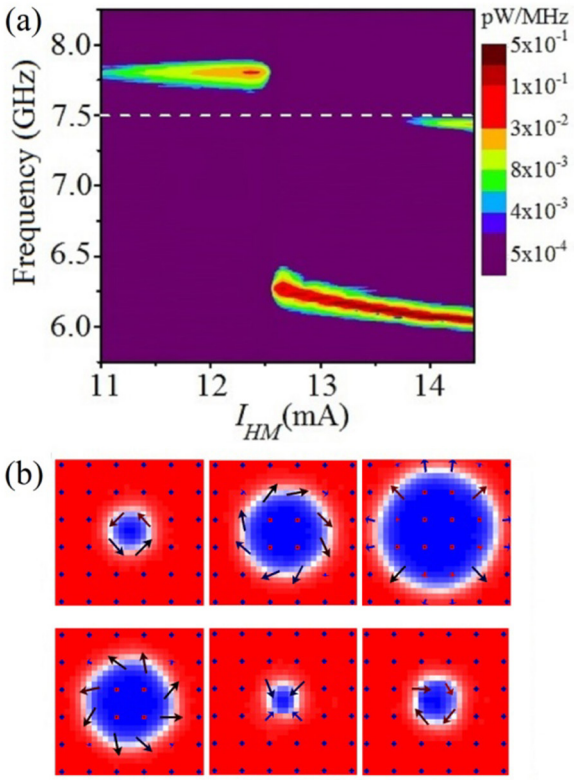

Figure 14. (a) Experimental frequency spectra as a function of the electrical current when the external perpendicular field is 110 mT, in a Pt/(Co/Ni) multilayer from [51] with permission from the American Physical Society, Copyright 2015. The white dashed line indicates the ferromagnetic resonance frequency. Adapted with permission from [51]. Copyright 2016 by the American Physical Society. (b) Spatial distribution of the magnetization at consecutive time instants, as obtained by means of micromagnetic simulations, when the dynamical skyrmion is excited [52, 53]. The colors are linked to the out-of-plane component of the magnetization (blue negative, red positive). Adapted from [52] with permission from the Nature Publishing Group, Copyright 2015.

Liu *et al* [51] carried out an experiment on Pt/(Co/Ni) multilayer patterned into a disk. The electrical current is injected into the Pt heavy metal to give rise to the SHE, which is able to excite magnetization dynamics in the Co/Ni. The frequency-current spectrum (see figure 14(a)) points out that different modes are generated. Above the FMR frequency, the dynamics is associated to a Slonczewski propagating mode [141] and exhibits a small blue-shift. Below the FMR, the frequency shows a red-shift, linked to the excitation of a bullet mode [142]. However, very close to the FMR frequency, another mode appears, which is identified, by means of micromagnetic simulations, as a dynamical skyrmion (limit cycle in presence of a sufficiently strong *i*-DMI). The spatial distribution of the magnetization highlights that the dynamical skyrmion is characterized by a 360° rotation of the in-plane spins of the domain wall, seen as a continual transformation from a Néel to Bloch skyrmion and vice versa.

Later, Zhou *et al* [52] micromagnetically and analytically analyzed a point-contact spin-valve. They showed that the dynamical skyrmion is characterized by a breathing of the skyrmion core at the same frequency of the domain wall dynamics (see figure 14(b)). The breathing causes a strong variation of the perpendicular magnetization m_z that allows to exploit the full magnetoresistance signal of the device. The dynamical skyrmion is expected to generate an output power of one order of magnitude larger than the one of droplets, since in the latter, only the domain wall spins contribute to the dynamics.

Recently [53], micromagnetic simulations have also pointed out the identification of a dynamical state, named instanton droplet (ID), in a *i*-DMI parameter—current phase diagram (see figure 15(a)). This mode is characterized by a continuous time domain transition between non-topological droplet (NTD) and a topological droplet (TD) (which has been also named the dynamical skyrmion in [52]). The term non-topological or topological used in [53] refers to the value of the skyrmion number, 0 or 1, of the limit cycle related to the NTD and TD dynamical state respectively. In other words, the ID is characterized by a time-dependent magnetization configuration connecting different topological states (TD and NTD), and a time-varying topological charge (skyrmion number), from TD ($|S| = 1$) to NTD ($S = 0$) and vice versa. The continual changes in the droplet topology generate incoherent emission of spin waves [53, 143].

A different skyrmion based spin-torque nano-oscillator can be realized as micromagnetically described by Zhang *et al* [144]. In particular, in a point-contact with circular geometry (see figure 15(b)), a force coming from the perpendicular spin-polarized current drives the skyrmion outside of the nanocontact region with a spiral trajectory, and finally the

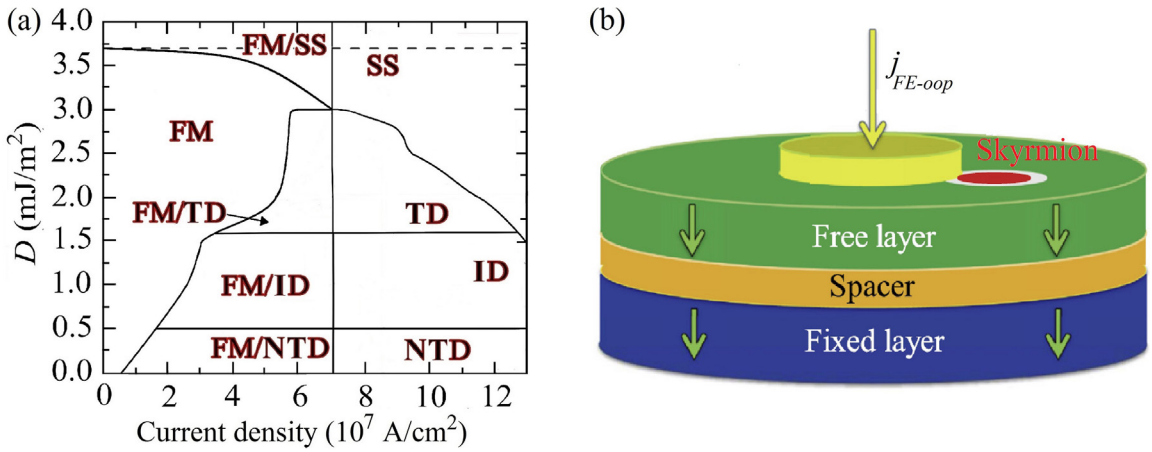

Figure 15. (a) Stability phase diagram of the magnetization ground-state as a function of the current density and D at zero external field from [53] Nature Publishing Group, Copyright 2015. The acronyms meaning is: FM: ferromagnetic; SS: static skyrmion; TD: topological droplet; NTD: non-topological droplet, ID: instanton droplet. (b) Sketch of the device where the skyrmion rotates around the nano-contact from [144] under the CC BY 3.0 license. The green arrows indicate the magnetization orientation.

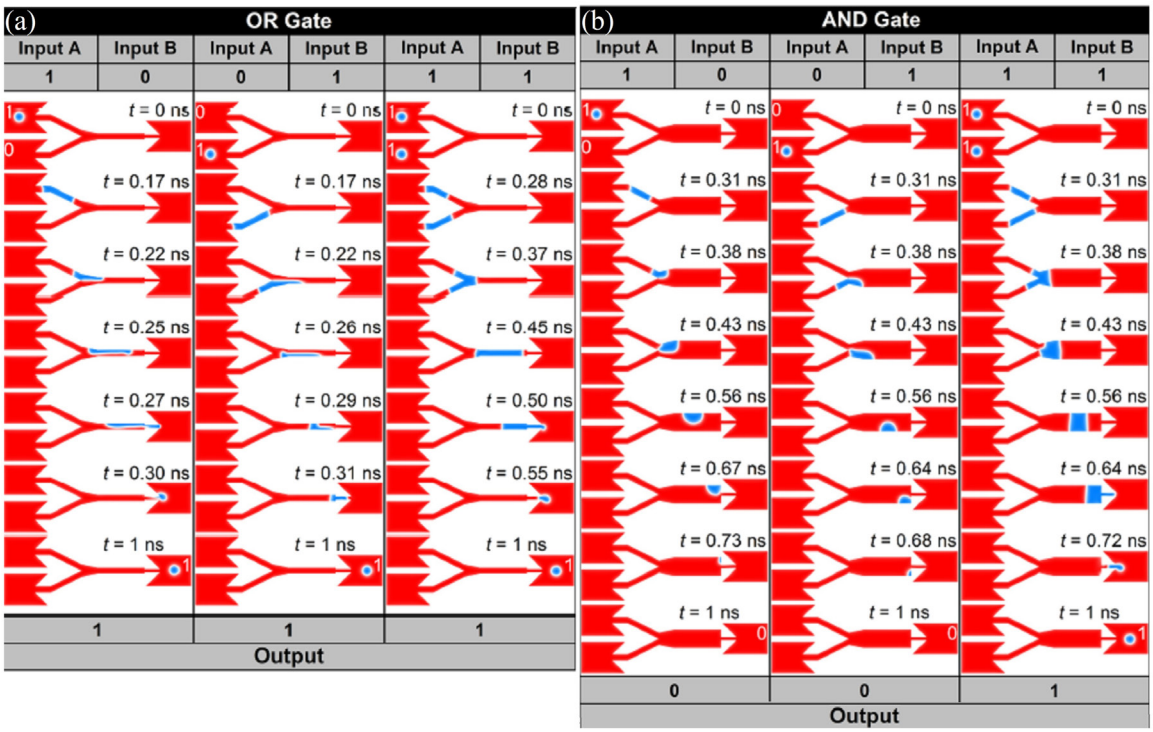

Figure 16. Examples of (a) OR and (b) AND logic gates based on skyrmions [145]. Adapted from [145] under the CC BY 4.0 license in Scientific Reports (Nature Publishing Group), Copyright 2016.

skyrmion reaches a persistent oscillation around the injection site of the current. The dynamics of the translational motion of the skyrmion is well-described by using the approach developed by Thiele [97]. Theoretically, the working frequency can be adjusted by the current density, radius of the nano-contact, and radius of the nano-disk. However, the output power of this solution is rather small as the magnetization below the contact stays almost constant during the skyrmion rotation.

6.3. Spin logic gates

The design of spin logic gates, such as the AND and OR gates based on the manipulations of skyrmions has been proposed in [145]. The OR gate is an operation such that $0 + 0 = 0$, $0 + 1 = 1$, $1 + 0 = 1$ and $1 + 1 = 1$. In skyrmionic logic, binary 0 corresponds to the absence of a skyrmion and binary 1 corresponds to the presence of a skyrmion. The schematic process is shown in figure 16. The case of $0 + 0 = 0$ is trivial, which means that when there is no input, there is no output. The processes $1 + 0 = 1$ $(0 + 1 = 1)$ can be interpreted as follows. When a skyrmion exists in one of the branches and there is no skyrmion in the other branch, one skyrmion is injected to the output nanowire. The process $1 + 1 = 1$ can be implemented as follows. There is a skyrmion in both branches at the first stage. If a current is applied, only one skyrmion is ejected. The AND gate ($0 + 1 = 0$, $0 + 1 = 0$, $1 + 0 = 0$ and

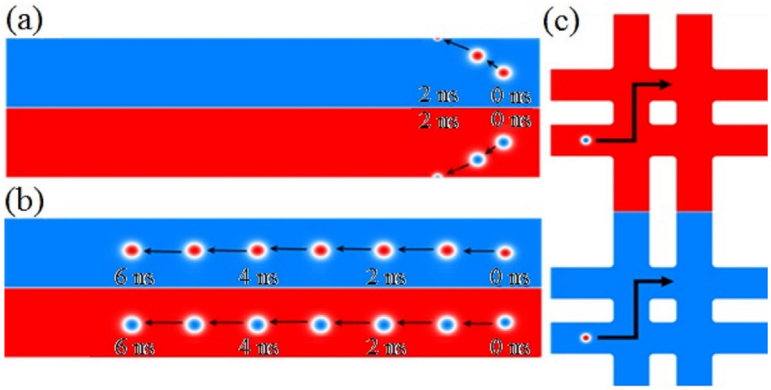

Figure 17. Skyrmion displacement in SAF structures. The contrast (red–blue) denotes the z-component of the magnetization. The upper part of the figure always represents a top-view of the magnetization in the bottom layer, whereas the lower part represents a top-view of the magnetization in the top layer. (a) Displacement of two skyrmions with opposite polarity in two uncoupled layers with opposite magnetization. The opposite Magnus force leads to an opposite skyrmion Hall effect resulting in both skyrmions moving to opposite edges of the wire, where they are, for a large enough driving force (current density), both expelled from the wire. (b) In case that both skyrmions are coupled, they move only along the wire with no skyrmion Hall effect. (c) For coupled skyrmions in a grid or matrix, the coupling that suppresses the skyrmion Hall effect allows the skyrmions to move around corners and in complex trajectories depending on the driving force.

$1 + 1 = 1$) can also be realized by using skyrmions. The process $0 + 0 = 0$ and $1 + 1 = 1$ are the same as that of the OR gate. For implementing the process $1 + 0 = 0$ or $0 + 1 = 0$, a skyrmion must disappear and there should be no output when a skyrmion exists only at one of the input branch. Essentially, if only one of the two input branches has a skyrmion, this skyrmion is converted into a meron in the central region, and disappears by touching the sample edge. Only if there are skyrmions in both input branches, these are converted into a DW pair, resulting in the output of one skyrmion. A limit for scalability of this approach results from the presence of edge roughness in real branches that can affect (local pinning centers) the DW motion achieved after the skyrmion conversion.

Finally, we want to point out that skyrmions hold great promise for logic and further applications as they can be moved on interconnected grids or matrices along complex trajectories as shown in figure 17. If layers are combined as SAFs, then the coupling between two skyrmions with antiparallel orientation in the two layers leads to the suppression of the skyrmion Hall effect and the skyrmions move along the driving force (for instance current flow, see figure 17(b)). In a complex grid or matrix arrangement, skyrmions can thus move around corners (see figure 17(c)), which is a major advantage over domain walls: for domain walls, the energy depends on the wall length and in a bifurcation or crossing, the wall length changes thus inevitably leading to a pinning site for the wall. For skyrmions, that do not touch the structure edge, this is not a problem and therefore skyrmions uniquely open the field of complex interconnected structures including bifurcations, crossings, dead-ends [35], etc. that can be used for very complex logic operations where the information can be transported as the number of skyrmions or even their geometrical arrangement. Finally, given the non-volatile nature of the magnetic systems, this uniquely leads to an inherent combination of logic and memory and thus could be useful for instant-on computing as well as low-power operation.

7. Summary and conclusions

Skyrmionics is a rapidly evolving field and this review can only provide a snapshot of the current state of the art. We have focused on the latest developments in the promising field of thin film skyrmionics, since the original work on skyrmions in B20 bulk compounds is covered by other excellent reviews already [31]. Skyrmions in thin film structures are particularly interesting for applications as these systems allow for scaling onto the nanoscale.

Specifically, we have discussed the topological nature of skyrmions, as well as their classification into Bloch and Néel skyrmions according to the type of DMI, the materials where they are stabilized and the corresponding spatial distribution of the magnetization. In the case of Bloch skyrmions, we have described the difference between chiral skyrmions and bubble skyrmions: the former is stabilized in presence of a large enough DMI, which fixes only one chirality of the skyrmion; the latter is obtained when the DMI does not a play a significant role. We have introduced the micromagnetic model based on the LLG equation for the analysis of the skyrmion properties, including also a brief description of the main torques used to manipulate skyrmions in multilayers, the related underlying physics, and the equation of motion based on Thiele's equation. We have discussed the basic features of skyrmions from a theoretical point of view in terms of stability, nucleation, annihilation, and characteristic dynamics, such as breathing and gyrotropic modes, as well as summarizing the latest experimental studies concerning the characterization of the skyrmion properties, such as field-dependence of the skyrmion diameter and measurements of the skyrmion Hall angle. Moreover, we have focused on the most important technological applications of skyrmions, i.e. the racetrack memory, from the first analytical and numerical investigations to the recent experimental evidence. Eventually, we have provided an overview of further potential applications of skyrmions in microwave detectors

and oscillators, and logic, which seem to be very promising according to recent micromagnetic results and predictions. In particular, unbiased detectors might exhibit a very large sensitivity, oscillators might increase the output power by exploiting the breathing mode of the 'dynamical skyrmion' and logic gates might take advantage of the 1D motion of skyrmions in synthetic antiferromagnets, where the skyrmion Hall effect is suppressed and thus complex skyrmion trajectories and devices are possible.

Acknowledgments

The authors thank the APS society, AAAS, AIP publishing, and Scientific Reports (Nature Publishing Group) for copyright permissions. GF, MC and RT acknowledge the bilateral agreement Italy-Turkey (TUBITAK-CNR) project (CNR Grant #B52I14002910005, TUBITAK Grant #113F378) 'Nanoscale magnetic devices based on the coupling of Spintronics and Spinorbitronics', and the executive programme of scientific and technological cooperation between Italy and China for the years 2016–2018 (code CN16GR09) title 'Nanoscale broadband spin-transfer-torque microwave detector' funded by Ministero degli Affari Esteri e della Cooperazione Internazionale. RT also acknowledges Fondazione Carit—Projects—'Sistemi Phased-Array Ultrasonori', and 'Sensori Spintronici'. M K thanks the German Science Foundation for funding through SPP 1538/SpinCaT, project BU 3297/1-1, and through SFB TRR 173/Spin+X. The authors are grateful for funding by the European Union through the EU-FP7 Marie Curie ITN WALL grant no. 608031, the H2020 ERC PoC MultiRev grant no. 665672, the Samsung SGMI program, the EFRE Program of the state of Rhineland Palatinate TT-DINEMA, the Excellence Graduate School MAINZ (GSC 266) and the state research centre CINEMA.
A large number of PhD students, postdocs and colleagues have contributed to the various aspects of this work and all their support, help and encouragement is gratefully acknowledged. In particular B Krüger and K Litzius are acknowledged for figure 17 as well as helpful discussions, and K Richter, R Reeve, A Krone and M Mawass for further support of the work. The authors thank Wanjun Jiang for the permission to use Figure 9(a) and Domenico Romolo for the graphical support.

References

[1] Remoissenet M 1994 *Waves Called Solitons: Concepts and Experiments* (Berlin: Springer)
[2] Khaykovich L, Schreck F, Ferrari G, Bourdel T, Cubizolles J, Carr L D, Castin Y and Salomon C 2002 *Science* **296** 1290
[3] Grelu P and Akhmediev N 2012 *Nat. Photon.* **6** 84
[4] Herr T, Brasch V, Jost J D, Wang C Y, Kondratiev N M, Gorodetsky M L and Kippenberg T J 2014 *Nat. Photon.* **8** 145
[5] Komarov A, Komarov K, Niang A and Sanchez F 2014 *Phys. Rev.* A **89** 013833
[6] Kläui M, Jubert P-O, Allenspach R, Bischof A, Bland J A C, Faini G, Rüdiger U, Vaz C A F, Vila L and Vouille C 2005 *Phys. Rev. Lett.* **95** 026601
[7] Parkin S S P, Hayashi M and Thomas L *Science* **320** 190
[8] Miron I M *et al* 2011 *Nat. Mater.* **10** 419
[9] Ryu K-S, Thomas L, Yang S H and Parkin S S P 2013 *Nat. Nanotech.* **8** 527
[10] Emori S, Bauer U, Ahn S-M, Martinez E and Beach G S D 2013 *Nat. Mater.* **12** 611
[11] Cowburn R P, Koltsov D K, Adeyeye A O and Welland M E 1999 *Phys. Rev. Lett.* **83** 1042
[12] Wachowiak A, Wiebe J, Bode M, Pietzsch O, Morgenstern M and Wiesendanger R 2002 *Science* **298** 577
[13] Yamada K, Kasai S, Nakatani Y, Kobayashi K, Kohno H, Thiaville A and Ono T 2007 *Nat. Mater.* **6** 270
[14] Pribiag V S, Krivorotov I N, Fuchs G D, Braganca P M, Ozatay O, Sankey J C, Ralph D C and Buhrman R A 2007 *Nat. Phys.* **3** 498
[15] Ruotolo A, Cros V, Georges B, Dussaux A, Grollier J, Deranlot C, Guillem R, Bouzehouane K, Fusil S and Fert A 2009 *Nat. Nanotech.* **4** 528
[16] Im M-Y, Fischer P, Yamada K, Sato T, Kasai S, Nakatani Y and Ono T 2012 *Nat. Commun.* **3** 983
[17] Giordano A, Puliafito V, Torres L, Carpentieri M, Azzerboni B and Finocchio G 2014 *IEEE Trans. Magn.* **50** 4300404
[18] Sluka V, Kákay A, Deac A M, Bürgler D E, Schneider C M and Hertel R 2015 *Nat. Commun.* **6** 6409
[19] Komineas S, Vaz C A F, Bland J A C and Papanicolau N 2005 *Phys. Rev.* B **71** 060405
[20] Vukadinovic N and Boust F 2007 *Phys. Rev.* B **75** 014420
[21] Ozatay O, Hauet T, Florez S H, Katine J A, Moser A, Thiele J-U, Folks L and Terris B D 2009 *Appl. Phys. Lett.* **95** 172502
[22] Makhfudz I, Kruger B and Tchernyshyov O 2012 *Phys. Rev. Lett.* **109** 217201
[23] Liu T, Puliafito V, Montaigne F, Petit S, Deranlot C, Andrieu S, Ozatay O, Finocchio G and Hauet T 2016 *J. Phys. D: Appl. Phys.* **49** 245002
[24] Rössler U K, Bogdanov A N and Pfleiderer C 2006 *Nature* **442** 797
[25] Bode M, Heide M, von Bergmann K, Ferriani P, Heinze S, Bihlmayer G, Kubetzka A, Pietzsch O, Blügel S and Wiesendanger R 2007 *Nature* **447** 190
[26] Mühlbauer S, Binz B, Jonietz F, Pfleiderer C, Rosch A, Neubauer A, Georgii R and Böni P 2009 *Science* **323** 915
[27] Yu X Z, Onose Y, Kanazawa N, Park J H, Han J H, Matsui Y, Nagaosa N and Tokura Y 2010 *Nature* **465** 901
[28] Heinze S, von Bergmann K, Menzel M, Brede J, Kubetzka A, Wiesendanger R, Bihlmayer G and Blügel S 2011 *Nat. Phys.* **7** 713
[29] Schulz T, Ritz R, Bauer A, Halder M, Wagner M, Franz C, Pfleiderer C, Everschor K, Garst M and Rosch A 2012 *Nat. Phys.* **8** 301
[30] Fert A, Cros V and Sampaio J 2013 *Nat. Nanotech.* **8** 152
[31] Nagaosa N and Tokura Y 2013 *Nat. Nanotech.* **8** 899
[32] Iwasaki J, Mochizuki M and Nagaosa N 2013 *Nat. Nanotech.* **8** 742
[33] Sampaio J, Cros V, Rohart S, Thiaville A and Fert A 2013 *Nat. Nanotech.* **8** 839
[34] Tomasello R, Martinez E, Zivieri R, Torres L, Carpentieri M and Finocchio G 2014 *Sci. Rep.* **4** 6784
[35] Zhang X, Zhao G P, Fangohr H, Liu J P, Xia W X, Xia J and Morvan F J 2015 *Sci. Rep.* **5** 7643
[36] Büttner F *et al* 2015 *Nat. Phys.* **11** 225
[37] Jiang W *et al* 2015 *Science* **349** 283
[38] Moreau-Luchaire C *et al* 2016 *Nat. Nanotech.* **11** 444–8
[39] Boulle O *et al* 2016 *Nat. Nanotech.* **11** 449
[40] Woo S *et al* 2016 *Nat. Mater.* **15** 501
[41] Landau L D and Lifshitz E 1935 *Phys. Z. Sowjetunion* **8** 153
[42] Gilbert T L 1955 *Phys. Z. Sowjetunion* **100** 1243
[43] Gilbert T L 2004 *IEEE Trans. Magn.* **40** 3443
[44] Komineas S 2012 *Europhys. Lett.* **98** 57002

[45] Hoefer M A, Silva T J and Keller M W 2010 *Phys. Rev.* B **82** 054432
[46] Mohseni S M *et al* 2013 *Science* **339** 1295
[47] Finocchio G, Puliafito V, Komineas S, Torres L, Ozatay O, Hauet T and Azzerboni B 2013 *J. Appl. Phys.* **114** 163908
[48] Macià F, Backes D and Kent A D 2014 *Nat. Nanotech.* **9** 992
[49] Puliafito V, Torres L, Ozatay O, Hauet T, Azzerboni B and Finocchio G 2014 *J. Appl. Phys.* **115** 17D139
[50] Puliafito V, Siracusano G, Azzerboni B and Finocchio G 2014 *IEEE Magn. Lett.* **5** 3000104
[51] Liu R H, Lim W L and Urazhdin S 2015 *Phys. Rev. Lett.* **114** 137201
[52] Zhou Y, Iacocca E, Awad A A, Dumas R K, Zhang F C, Braun H B and Åkerman J 2015 *Nat. Commun.* **6** 8193
[53] Carpentieri M, Tomasello R, Zivieri R and Finocchio G 2015 *Sci. Rep.* **5** 16184
[54] Slonczewski J C 1996 *J. Magn. Magn. Mater.* **159** L1
[55] Moutafis C, Komineas S and Bland J A C 2009 *Phys. Rev.* B **79** 224429
[56] Braun H B 2012 *Adv. Phys.* **61** 1
[57] Büttner F 2013 Topological mass of magnetic Skyrmions probed by ultrafast dynamic imaging *PhD Dissertation* University of Mainz, Mainz
[58] Chen G, Mascaraque A, N'Diaye A T and Schmid A K 2015 *Appl. Phys. Lett.* **106** 242404
[59] Dzyaloshinskii I 1958 *J. Phys. Chem. Solids* **4** 241
[60] Moriya T 1960 *Phys. Rev. Lett.* **4** 228
[61] Huang S X and Chien C L 2012 *Phys. Rev. Lett.* **108** 267201
[62] Brown W F 1963 *Micromagnetics* (New York: Wiley)
[63] Aharoni A 1996 *Introduction to the Theory of Ferromagnetism* (New York: Oxford University Press)
[64] Hubert A and Schäfer R 1998 *Magnetic Domains* (Berlin: Springer)
[65] Bertotti G 1998 *Hysteresis in Magnetism—for Physicists, Materials Scientists and Engineers* (New York: Academic)
[66] Lopez-Diaz L *et al* 2012 *J. Phys. D: Appl. Phys.* **45** 323001
[67] Rohart S and Thiaville A 2013 *Phys. Rev.* B **88** 184422
[68] Tomasello R, Carpentieri M and Finocchio G 2014 *J. Appl. Phys.* **115** 17C730
[69] Åkerman J 2005 *Science* **308** 508
[70] Zeng Z, Finocchio G and Jiangc H 2013 *Nanoscale* **5** 2219
[71] Berger L 1996 *Phys. Rev.* B **54** 9353
[72] Hirsch J E 1999 *Phys. Rev. Lett.* **83** 1834
[73] Hoffmann A 2013 *IEEE Trans. Magn.* **49** 5172
[74] Slavin A and Tiberkevich V 2009 *IEEE Trans. Magn.* **45** 1875
[75] Slonczewski J 2005 *Phys. Rev.* B **71** 024411
[76] Sankey J C, Cui Y-T, Sun J Z, Slonczewski J C, Buhrman R A and Ralph D C 2008 *Nat. Phys.* **4** 67
[77] Liu L, Pai C-F, Li Y, Tseng H W, Ralph D C and Buhrman R A 2012 *Science* **336** 555
[78] Demidov V E, Urazhdin S, Ulrichs H, Tiberkevich V, Slavin A, Baither D, Schmitz G and Demokritov S O 2012 *Nat. Mater.* **11** 1028
[79] Liu L, Pai C-F, Ralph D C and Buhrman R A 2012 *Phys. Rev. Lett.* **109** 186602
[80] Sinova J, Valenzuela S O, Wunderlich J, Back C H and Jungwirth T 2015 *Rev. Mod. Phys.* **87** 1213
[81] Finocchio G, Carpentieri M, Martinez E and Azzerboni B 2013 *Appl. Phys. Lett.* **102** 212410
[82] Tomasello R, Carpentieri M and Finocchio G 2013 *Appl. Phys. Lett.* **103** 252408
[83] Giordano A, Carpentieri M, Laudani A, Gubbiotti G, Azzerboni B and Finocchio G 2014 *Appl. Phys. Lett.* **105** 042412
[84] Puliafito V, Giordano A, Azzerboni B and Finocchio G 2016 *J. Phys. D: Appl. Phys.* **49** 145001
[85] Garello K, Miron I M, Avci C O, Freimuth F, Mokrousov Y, Blügel S, Auffret S, Boulle O, Gaudin G and Gambardella P 2013 *Nat. Nanotech.* **8** 587
[86] Brataas A and Hals K M D 2014 *Nat. Nanotech.* **9** 86
[87] Haney P M, Lee H-W, Lee K-J, Manchon A and Stiles M D 2013 *Phys. Rev.* B **87** 17441
[88] Freimuth F, Blügel S and Mokrousov Y 2014 *Phys. Rev.* B **90** 174423
[89] Zhang S and Li Z 2004 *Phys. Rev. Lett.* **93** 127204
[90] Tataraa G, Kohnoc H and Shibatad J 2008 *Phys. Rep.* **468** 213
[91] Boulle O, Malinowskib G and Kläui M 2011 *Mater. Sci. Eng.* R **72** 159
[92] Maruyama T *et al* 2009 *Nat. Mater.* **4** 158
[93] Wang W-G, Li M, Hageman S and Chien C L 2012 *Nat. Mater.* **11** 64
[94] Zhu J *et al* 2012 *Phys. Rev. Lett.* **108** 197203
[95] Carpentieri M, Tomasello R, Ricci M, Burrascano P and Finocchio G 2014 *IEEE Trans. Magn.* **50** 140804
[96] Kang W, Huang Y, Zheng C, Lv W, Lei N, Zhang Y, Zhang X, Zhou Y and Zhao W 2016 *Sci. Rep.* **6** 23164
[97] Thiele A A 1972 *Phys. Rev. Lett.* **30** 230
[98] Thiaville A, Nakatani Y, Miltat J and Suzuki Y 2005 *Europhys. Lett.* **69** 990
[99] Everschor K, Garst M, Duine R A and Rosch A 2011 *Phys. Rev.* B **84** 064401
[100] Schütte C, Iwasaki J, Rosch A and Nagaosa N 2014 *Phys. Rev.* B **90** 174434
[101] Zhou Y and Ezawa M 2014 *Nat. Commun.* **5** 4652
[102] Romming N, Hanneken C, Menzel M, Bickel J E, Wolter B, von Bergmann K, Kubetzka A and Wiesendanger R 2013 *Science* **341** 636
[103] Romming N, Kubetzka A, Hanneken C, von Bergmann K and Wiesendanger R 2015 *Phys. Rev. Lett.* **114** 177203
[104] Ma F, Ezawa M and Zhou Y 2015 *Sci. Rep.* **5** 15154
[105] Giordano A *et al* 2016 arXiv:1606.07280
[106] Lin S-Z, Batista C D and Saxena A 2014 *Phys. Rev.* B **89** 024415
[107] Kim J V, Garcia-Sanchez F, Sampaio J, Moreau-Luchaire C, Cros V and Fert A 2014 *Phys. Rev.* B **90** 064410
[108] Finocchio G, Ricci M, Tomasello R, Giordano A, Lanuzza M, Puliafito V, Burrascano P, Azzerboni B and Carpentieri M 2015 *Appl. Phys. Lett.* **107** 262401
[109] Onose Y, Okamura Y, Seki S, Ishiwata S and Tokura Y 2012 *Phys. Rev. Lett.* **109** 037603
[110] Schwarze T, Waizner J, Garst M, Bauer A, Stasinopoulos I, Berger H, Pfleiderer C and Grundler D 2015 *Nat. Mater.* **14** 478
[111] Mochizuki M 2012 *Phys. Rev. Lett.* **108** 017601
[112] Moon K-W, Chun B S, Kim W, Qiu Z Q and Hwang C 2014 *Phys. Rev.* B **89** 064413
[113] Malozemoff A P and Slonczewski J C 1979 *Magnetic Domain Walls in Bubble Materials* (New York: Academic)
[114] Yu X, Mostovoy M, Tokunaga Y, Zhang W, Kimoto K, Matsui Y, Kaneko Y, Nagaosa N and Tokura Y 2012 *Proc. Natl Acad. Sci.* **109** 8856
[115] Mochizuki M, Yu X Z, Seki S, Kanazawa N, Koshibae W, Zang J, Mostovoy M, Tokura Y and Nagaosa N 2014 *Nat. Mater.* **13** 241
[116] Yamasaki Y, Morikawa D, Honda T, Nakao H, Murakami Y, Kanazawa N, Kawasaki M, Arima T and Tokura Y 2015 *Phys. Rev.* B **92** 220421
[117] Büttner F *et al* 2013 *Phys. Rev.* B **87** 134422
[118] Kézsmárki I *et al* 2015 *Nat. Mater.* **14** 1116
[119] Neubauer A, Pfleiderer C, Binz B, Rosch A, Ritz R, Niklowitz P G and Böni P 2009 *Phys. Rev. Lett.* **102** 186602
[120] Jonietz F *et al* 2010 *Science* **330** 1648
[121] Jiang W *et al* 2016 arXiv:1603.07393
[122] Milde P *et al* 2013 *Science* **340** 1076
[123] Yu G, Upadhyaya P, Li X, Li W, Kim S K, Fan Y, Wong K L, Tserkovnyak Y, Amiri P K and Wang K L 2016 *Nano Lett.* **16** 1981
[124] Kiselev N S, Bogdanov A N, Schäfer R and Rössler U K 2011 *J. Phys. D: Appl. Phys.* **44** 392001

[125] Kiselev N S, Bogdanov A N, Schäfer R and Rössler U K 2011 *Phys. Rev. Lett.* **107** 179701
[126] Yu X Z, Kanazawa N, Zhang W Z, Nagai T, Hara T, Kimoto K, Matsui T, Onose Y and Tokura Y 2012 *Nat. Commun.* **3** 988
[127] Iwasaki J, Mochizuki M and Nagaosa N 2013 *Nat. Commun.* **4** 1463
[128] Everschor K, Garst M, Binz B, Jonietz F, Mühlbauer S, Pfleiderer C and Rosch A 2012 *Phys. Rev.* B **86** 054432
[129] Zhang X, Zhou Y and Ezawa M 2016 *Nat. Commun.* **7** 10293
[130] Yang S-H, Ryu K-S and Parkin S S P 2015 *Nat. Nanotech.* **10** 221
[131] Parkin S S P and Mauri D 1991 *Phys. Rev.* B **44** 7131
[132] Tulapurkar A A, Suzuki Y, Fukushima A, Kubota H, Maehara H, Tsunekawa K, Djayaprawira D D, Watanabe N and Yuasa D 2005 *Nature* **438** 339
[133] Sankey J C, Braganca P M, Garcia A G F, Krivorotov I N, Buhrman R A and Ralp D C 2006 *Phys. Rev. Lett.* **96** 227601
[134] Kubota H *et al* 2008 *Nat. Phys.* **4** 37
[135] Ishibashi S *et al* 2011 *IEEE Trans. Magn.* **47** 3373
[136] Wang C, Cui Y-T, Sun J Z, Katine J A, Buhrman R A and Ralph D C 2009 *J. Appl. Phys.* **106** 053905
[137] Cheng X, Boone C T, Zhu J and Krivorotov I N 2010 *Phys. Rev. Lett.* **105** 047202
[138] Miwa S *et al* 2014 *Nat. Mater.* **13** 50
[139] Fang B *et al* 2016 *Nat. Commun.* **7** 11259
[140] Meng H, Sbiaa R, Akhtar M A K, Liu R S, Naik V B and Wang C C 2012 *Appl. Phys. Lett.* **100** 122405
[141] Slonczewski J C 1999 *J. Magn. Magn. Mat.* **195** L261
[142] Bonetti S, Tiberkevich V, Consolo G, Finocchio G, Muduli P, Mancoff F, Slavin A and Åkerman J 2010 *Phys. Rev. Lett.* **150** 217204
[143] Schütte C and Garst M 2014 *Phys. Rev.* B **90** 094423
[144] Zhang S, Wang J, Zheng Q, Zhu Q, Liu X, Chen S, Jin C, Liu Q, Jia C and Xue D 2015 *New J. Phys.* **17** 023061
[145] Zhang X, Ezawa M and Zhou Y 2015 *Sci. Rep.* **5** 9400